University of Bergen

Master's Thesis in Physical Oceanography

Numerical modelling of the sub-surface melting of marine-terminating glaciers in Arctic fjords

Author:
Kjersti Kalhagen

Supervisors:
Lars Asplin, IMR
Paul Budgell, IMR
Frank Nilsen, UNIS, UiB

June 2015

Acknowledgements

I would like to thank my main supervisor Lars for teaching me alot about fjord modelling, programming, oceanography, long-forgotten physics, and of course salmon lice, for helpful discussions, and most of all for staying positive and optimistic when I was being a superpessimist. I also appreciate being able to visit the Fram Centre in Tromsø – twice, even – where I got to meet many talented researchers. Also thanks for the opportunity to go to Flødevigen for a cruise, which was a well-needed break from Geofysen. And finally thanks for reading almost uncountably many frustration-filled emails and editions of the thesis, providing corrections and advice on improvement.

I also thank my second supervisor Paul for sharing his knowledge about how to handle the ice-melt model, helping me to understand the difficult aspects of modelling plume dynamics and submarine melting, for giving new ideas, for presenting some temporary results to the researchers at Woods Hole Oceanographic Institution, and for taking time to error-search via e-mail when things just wouldn't work.

My third supervisor Frank has been a great course-leader in the Air–Sea–Ice Interactions courses at the University Centre in Svalbard. The five-week long course in the Autumn of 2014 was equally much an intensive time with fieldwork, studying, and report-writing as it was a good vacation from the normal life in the mainland. New insights made me keep interest in the studies, and I came back with new energy to work further. I am also grateful for comments on the thesis and many encouraging words before the deadline.

I am also thankful for good advice, helpful discussions, and fun stories (and coffee) from the researchers at the Institute of Marine Research.

I appreciate the lunch breaks and even longer afternoon coffee breaks with the fellow students at Geofysen. Long days and nights of working had not been possible without breaks with silly discussions.

Stefanie and Sebastian deserve special thanks for the time they spent reading some of my text and making suggestions on how to improve it. I am also very grateful for all the support, positive words, lots of encouragement, and funny notes on my desk from my name-sister Kjersti.

Abstract

Submarine melting of glaciers terminating in fjords is likely to be of high importance regarding the total ice loss from ice sheets and ice caps and the resulting addition of freshwater to the ocean. Submarine melting generates a buoyant plume which ascend along the calving front of the glacier and sets up a circulation. In addition, surface melt on the glacier drains to the bedrock and gets discharged at depth into the fjord. Earlier, this has been shown to further enhance the buoyancy-driven circulation near the glacier front. The buoyant plume entrains ambient warm fjord water as it ascends, and the circulation it sets up also drives warm fjord water toward the glacier front at depth in order to conserve volume. These processes replenish the near-glacier area with heat available for melting. The purpose of this study is to investigate the submarine melting of marine-terminating glaciers and the resulting buoyancy-driven circulation in fjords in Greenland. First the non-hydrostatic high-resolution Bergen Ocean Model is used in a series of simulations to reproduce earlier results obtained by the Massachusetts Institute of Technology general circulation model with a meltrate parameterization developed for melting beneath ice shelves in Antarctica. The simulated meltrates found in this study are in the range $43\,\mathrm{m\,yr^{-1}}$ to $1043\,\mathrm{m\,yr^{-1}}$. The melting at the glacier front is sensitive to oceanic thermal forcing following a linear relation and to discharge of surface runoff following a cubic root relation. Then, it is attempted to apply this modelling approach to glacial fjords in Svalbard. The modelled fjords in these simulations are shallower than the deep fjords of Greenland, and the consequences of smaller fjord depth are studied for various forcings. The meltrate ranges from $9\,\mathrm{m\,yr^{-1}}$ to $895\,\mathrm{m\,yr^{-1}}$, and its value is highly sensitive to subglacial discharge, the stratification of the fjord water and the rate of replenishment of warm ambient fjord water to the glacier front by the return current at depth.

Contents

Chapter 1

Introduction

1.1 Increased mass loss from the Greenland ice sheet

In the recent decades, the mass loss from the Greenland ice sheet has increased significantly. The mass loss in the years 2002–2011 of $211 \pm 37\,\mathrm{Gt\,yr^{-1}}$ is four times larger than that in 1992–2001 (Straneo and Heimbach, 2013). About one fourth of the observed global sea level rise is accounted for by the mass loss from the Greenland ice sheet and the Antarctic ice sheets (e.g. Straneo et al., 2013), of which the mass loss from Greenland is the largest. The increase in mass loss has been attributed to the negative surface mass balance due to increased surface melting in southeast and west Greenland, and to the many marine-terminating glaciers speeding up (Straneo et al., 2010), thinning and retreating, causing an increase in ice discharge (Straneo and Heimbach, 2013). Observations of the Kangerdlugssuaq Glacier and the Helheim Glacier on the east coast of Greenland have shown retreats of the glacier fronts much greater than the previously observed seasonal fluctuations. These large retreats occurred after a period of ice thinning and coincided with an accelerated ice flow. During these years, the increased mass loss rates for the Kangerdlugssuaq and Helheim Glaciers represented almost half of the increase of mass loss of the Greenland ice sheet (Howat et al., 2007).

1.2 Acceleration of outlet glaciers

The acceleration of the outlet glaciers in Greenland is suggested to be caused by increased melting at the ice–ocean interface driven by warming of subtropical waters offshore Greenland (Straneo et al., 2010), although there is a complex spatial and temporal variability in the acceleration of the glaciers, suggesting they are influenced by a combination of forcings (Moon et al., 2012; Straneo et al., 2013). Changes in the North Atlantic

Ocean impact the glaciers of Greenland within a year, and changes in the volume and properties of the subtropical water on the shelf affect the melting of the tidewater glacier fronts (Straneo et al., 2010).

1.3 Uncertainty in predictions of ice loss and sea level rise

The dynamics of tidewater glaciers and ice sheet stability are directly affected by increased surface ablation and higher ocean temperatures. In addition, Motyka et al. (2013) have shown that an increasing fjord circulation near the glacier fronts also affect glacier dynamics and ice sheet stability. The circulation near the glacier termini is partially driven by glacial runoff (Motyka et al., 2013, 2003), which has been shown to have a large impact on the melting on the marine-terminating glacier fronts (Jenkins, 2011; Kimura et al., 2014; Sciascia et al., 2013).

As there are major uncertainties regarding the interaction between ice sheets and the ocean in predicting future ice loss and sea level rise (Motyka et al., 2013; Straneo et al., 2013), it is essential to study these interactions in greater detail (Rignot et al., 2010).

Submarine melting have a large influence on grounding-line stability and ice-flow dynamics (Rignot et al., 2010), and it has been shown that the termini of tidewater glaciers have seasonal variability coinciding with changes in freshwater discharged at depth and fjord water temperatures, which suggests that glacier front fluctuations are directly related to variability in submarine melting (Motyka et al., 2003).

1.4 Oceanographic forcing on submarine melting

The submarine melting of glacier termini is caused by warm water masses being present in the vicinity of the termini (Xu et al., 2013), and warm water of Atlantic origin is recognized as contributing to the increasing ice loss from the Greenland ice sheet (Inall et al., 2014).

Oceanographic data collected in the Sermilik Fjord in July and September 2008 show the presense of subtropical waters throughout the fjord and that these waters gets continuously replenished through wind-driven exchange with the shelf water (Straneo et al., 2010). Several surveys have revealed that Greenland fjords have a capping layer of cold and fresh Arctic waters (PW) above the warmer and more saline water of Atlantic origin (e.g. Straneo et al., 2011, 2010).

The properties of the fjord water in Greenland fjords can vary within few days. In addition to surveys done in the summer months, there are available continuous records of water properties and velocity in the winter months between September and May. Jackson et al. (2014) have shown that although PW and AW are always present (in the Sermilik fjord), the water properties and overall heat content in the Sermilik and Kangerdlugssuaq fjords vary significantly over days due to rapid water exchange with shelf water during the winter months. The frequent and rapid velocity pulses drive external water masses into the fjords and renew the warm water faster than the glacially driven circulation. Jackson et al. (2014) attribute the pulses to intermediary circulation, which is the term for a pumping mechanism driven by density fluctuations at the fjord mouth, and show evidence for the existence of this circulation which has been hypothesized as being important (Straneo et al., 2010). Also associated to the pulses are winds on the shelf that favour downwelling. Jackson et al. (2014) also speculate that occational pulses can be forced without wind – that shelf–fjord pressure gradients may be generated by phenomena like coastally trapped waves or AW eddies.

Seasonal trends include a general deepening and cooling of the PW layer in the winter. Changes in the depth of the interface between the layers can also fluctuate over a few days. Jackson et al. (2014) argue that the variability in the properties of the fjord water is primarily due to exchange with the shelf and not internal mixing and surface fluxes: internal mixing would reduce the stratification and redistribute the heat, which is not the case as the Sermilik fjord has a persistent stratification, and surface fluxes would cool the water and also reduce the stratification.

1.5 Subglacial discharge as a driver of submarine melting and fjord circulation

The melting of the submarine glacier termini is dependent on the heat content of the fjord water, but in order for the warm water masses to affect the glacier fronts, the available heat in the fjord must be transported toward the fronts (Motyka et al., 2013). There is a lack of understanding of how the heat content of the water masses in the fjords is communicated to the glacier fronts (Inall et al., 2014). The circulation within the fjords is governed by several processes arising from external forcing as wind stress, tidal currents, and exchanges with the shelf (Straneo et al., 2011). Additionally there is circulation driven by the glacier itself, which is thought to be the dominant circulation in the vicinity of the glacier (Sciascia et al., 2013) and has been shown to impact the melting of the glacier fronts (Jenkins, 2011; Kimura et al., 2014; Sciascia et al., 2013).

This circulation is buoyancy-driven and arises due to submarine melting at the glacier front but is also forced by freshwater discharged at depth. The freshwater which is discharged into the fjord at depth is the portion of the snow, firn and glacier ice which has melted on the surface of the glacier in the catchment basin, drained through crevasses and moulins, reached the bed rock beneath the glacier and discharged into the fjord at the grounding line (Sciascia et al., 2013; Xu et al., 2013).

By the glacier front, a buoyant plume will rise along the vertical ice front due to the subglacial discharge near the bottom and submarine melting of the ice front. As it ascends it entrains ambient warmer water, so the resulting buoyant current is a mix of water of glacial origin and of warm, saline fjord water. The entrainment of ambient fjord water into the buoyant plume leads heat to the glacier ice and enhances the melting.

The plume ascends until it has reached the depth at which the plume density matches the ambient density. The plume density is dependent on the balance between the rate at which the plume melts glacier ice at the front and the rate of entrainment of fjord water. These also depend on each other. For instance will a large submarine meltrate decrease the plume density and thus make it more buoyant. That will in turn make the plume accelerate upwards, and as a consequence it will entrain more ambient water which again will lower the plume buoyancy. On the other hand will large entrainment of fjord water increase the plume density and make it less buoyant due to the high salinity. But it will also lead more heat to the glacier ice so that the submarine melting is enhanced, which then will increase the buoyancy.

When the plume reaches its neutral density level, which may be surface level, the glacially modified water will flow horizontally away from the glacier front. This current of relatively fresh water will cause a return flow at depth in order to conserve volume. Due to the temperature difference between the relatively cold outflow of glacially modified water and the warm ambient fjord water, this circulation yields a net heat transport toward the glacier front.

1.6 Previous work

Estimation of submarine meltrates of glacier fronts has been done by observing water properties and currents to calculate heat transport toward the glaciers (e.g. Inall et al., 2014; Rignot et al., 2010; Sutherland and Straneo, 2012).

There has also been extensive numerical modelling of the submarine melting of floating ice shelves in Antarctica (e.g. Hellmer and Olbers, 1989; Holland and Jenkins, 1999;

Holland et al., 2008). These models are based on heat and freshwater fluxes associated with phase changes at the ice–ocean boundary.

Modelling of the melting of tidewater glaciers on the other hand is less extensive. Focusing on marine-terminating glaciers with a vertical front was motivated when it was found that the conventional parameterizations of ice–ocean heat transfer could not account for the high meltrates of the LeConte Glacier in Alaska (Jenkins, 2011; Motyka et al., 2003), suggesting the high meltrates were enhanced by surface freshwater discharged at depth and the following convection along the ice front (Kimura et al., 2014).

Submarine melting of marine-terminating glacier fronts have been modelled by using one-dimensional plume models (Jenkins, 2011), fine-resolution general circulation models (GCM) with a two-dimensional domain (vertical and along-fjord) and a melting model implemented on the vertical glacier front (e.g. Sciascia et al., 2013; Xu et al., 2012), and full three-dimensional GCM which allows for across-fjord currents and across-fjord variations in freshwater addition at depth and submarine melting (e.g. Cowton et al., 2015; Xu et al., 2013).

1.7 Overall goal of the thesis

Due to the importance this buoyancy-driven circulation has on the melting of marine-termining glacier fronts and the large uncertainties in the interaction between the glacier fronts and the ocean regarding the prediction of future ice loss and sea level rise, we aim to study these processes and gain insight in the complex system.

In idealized model simulations, we study the buoyancy-driven circulation in a glacial fjord in absense of external forcings such as wind stress, tidal currents, rotational dynamics, and fjord–shelf interaction. The goal is to obtain probable ranges of submarine meltrate of the glacier front and how this meltrate depends on various forcings – the amount of freshwater discharged into the fjord at depth, various fjord water properties, fjord depth and stratification.

As a first step, we aim to reproduce the results obtained by Sciascia et al. (2013) for the Helheim Glacier–Sermilik Fjord system to see whether differences between the models make a significant impact on the results. Sciascia et al. (2013) used the general circulation model at the Massachusetts Institute of Technology (MITgcm) with a high-resolution, non-hydrostatic setup. The MITgcm solves the Boussinesq form of the Navier–Stokes equations and renders the finite-volume discretization on an Arakawa C-grid with vertical z-levels. Sciascia et al. (2013) modelled submarine melting and fjord circulation in a vertical slice of the fjord, i.e., in the vertical and along-fjord directions as

it was found that there was no significant across-fjord variability and that the differences between two-dimensional slice and full three-dimensional domain were small. Using a two-dimensional setup has the advantage of reduced computational costs.

In this study, we use the Bergen Ocean Model (BOM) and use a setup which is as similar as possible to the setup of the MITgcm simulations of Sciascia et al. (2013). Some differences were inevitable, however. We use a grid which is everywhere uniform, in contrast to Sciascia et al. (2013) who has a telescoping resolution in the along-fjord direction. The telescoping resolution in MITgcm, which ranges from 10 m at the glacier front to 500 m at the fjord mouth 160 km away, gives identical resolution at the glacier front and only small differences to our uniform resolution in the area of the domain we study. Thus, the difference in the along-fjord resolution is assumed to not give results which are significantly different. Also, BOM has sigma-coordinates in the vertical, but since the bottom is flat, this corresponds to vertical z-levels so that overall, the resolution in the near-glacier domain in BOM are as similar as possible to that in MITgcm. Another difference between the models that could not be avoided but is more likely to have an impact on the results is the boundary conditions. Sciascia et al. (2013) used no-slip conditions at the rigid boundaries, i.e., on the bottom and on the glacier front. A no-slip condition could not be used in BOM, and attempts to use a partial-slip condition at the rigid boundaries did not give probable results as the meltrate formulations in the ice model does not take into account variability in the plume position relative to the glacier front and variability in the boundary layer length. Thus, we perform all simulations with a free-slip condition at the rigid boundaries. It can be argued that free-slip conditions are more physically correct to use at the glacier front boundary as glacier ice is smooth compared to land boundaries. However, we cannot conclude on which condition is the more correct to use as there are few observations of how the structure of the glacier front is and how the plume velocities is altered at the boundary due to the structure of the ice front. By observing the recently calved ice bergs, it has been found that at the glacier front, there are half-cylindrical patterns created by plume interactions and cusps in areas where there is submarine melting which is not forced by a plume (Powell, 2012). According to Kimura et al. (2014), the character of the plume and therefore also the meltrate is critically dependent on the velocity boundary conditions at the wall. This was found by using a free-slip condition, a weakly applied no-slip condition, and a quadratic drag, in simulations without meltwater feedback. They found that with a no-slip condition applied, the meltrate is reduced due to a reduction of the vertical velocity near the ice face. The drag condition gave results close to those with the free-skip condition. Kimura et al. (2014) also argues that it is not justified to apply no-slip conditions when the boundary layer turbulence is not fully resolved. Apart from these differences between MITgcm and BOM, the setups are similar.

After the reproduction of the Helheim Glacier–Sermilik Fjord system results of Sciascia et al. (2013), we continue by going more in depth on the relative importance of oceanic forcing (water temperature) and atmospheric forcing (volume flux of subglacial discharge resulting from warm air over the glacier). This covers scenarios in which the fjord water is warm in winter due to inflow of shelf waters and high-flux subglacial discharge into relatively cold fjord water.

We also model the buoyancy-driven circulation and submarine melting in fjords which are shallower. This is to find out if similar stratification and subglacial discharge rates give the same results in a shallow fjord as in the deep Sermilik Fjord. It will also be a first step in the process of including submarine melting of the tidewater glacier fronts in the high-resolution three-dimensional model simulations in the glacial fjords of Spitsbergen. We start with idealized simulations with a vertical two-dimensional slice to ascertain that this approach is suitable also for shallow fjords and to establish how the melting and circulation are likely to be in the shallower fjords of Spitsbergen compared to the deep fjords in Greenland which have gotten more attention in this field of study. The results of the idealized two-dimensional simulations can later be used to develop more complex three-dimensional modelling of the Spitsbergen glacier–fjord systems including bathymetry and external forcing. Several projects may benefit from the results in this study as a supplement to the existing three-dimensional circulation models or as a part of a foundation for coupled model systems. For instance are there plans to run the high-resolution non-hydrostatic version of BOM in the upper reaches of Kongsfjorden, Spitsbergen so that BOM supplies boundary conditions of subglacial discharge and submarine melting from the glacier front to a coarser-resolution circulation model in the fjord at some distance away from the glacier front.

Information about the Bergen Ocean Model is found in Chapter 2, along with a description of the ice model which is included for the submarine melting of the glacier front. There is also descriptions of parameters we use and an overview of the simulations performed. In Chapter 3, we present the results, and these are discussed and compared to other studies in Chapter 4. Finally, conclusion and summary is found in Chapter 5.

Chapter 2

Methods

2.1 Bergen Ocean Model

The Bergen Ocean Model (BOM) is a σ-coordinate numerical ocean model which solves the equations for momentum, continuity, and conservation of temperature and salinity and results in three-dimensional velocity, density, temperature, and salinity fields, among others. The discretization is rendered on a staggered Arakawa C-grid (Berntsen, 2000).

In this study, version 5.0 alpha5 is used (Bergen Ocean Model, 2014). This is the non-hydrostatic version of BOM. The model is modified to include an ice-melt model (Section 2.1.2).

2.1.1 Spatial resolution, time stepping, conditions for stability

The spatial resolution is uniform in the x-direction (along-fjord) and the y-direction (across-fjord). With a flat bottom, also the resolution in the vertical direction is uniform.

In order to avoid instabilities, the time step needs to be chosen to be small enough to satisfy the CFL-criterion, which for the shallow water equations is given by

$$C_{2D} = \delta t_{2D} \frac{1}{\delta x} \sqrt{2gH_{max}} \leq 1, \tag{2.1}$$

and for internal waves

$$C_{3D} = \delta t_{3D} \frac{1}{\delta x} \sqrt{2g'H_{max}} \leq 1, \tag{2.2}$$

Symbol	Description	Value	Unit
λ_1	Liquidus slope / salinity coefficient	-5.73×10^{-2}	°C
λ_2	Liquidus intercept / constant coefficient	8.32×10^{-2}	°C
λ_3	Liquidus slope / depth coefficient	7.61×10^{-4}	$°C\,m^{-1}$
$\sqrt{C_d}\,\Gamma_T$	Thermal Stanton number	1.1×10^{-3}	
$\sqrt{C_d}\,\Gamma_S$	Haline Stanton number	3.1×10^{-5}	
ν_H	Horizontal viscocity	2.5×10^{-1}	$m^2\,s^{-1}$
ν_V	Vertical viscocity	1.0×10^{-3}	$m^2\,s^{-1}$
κ_H	Horizontal diffusion	2.5×10^{-1}	$m^2\,s^{-1}$
κ_V	Vertical diffusion	2.0×10^{-5}	$m^2\,s^{-1}$
L_f	Latent heat of fusion of ice	3.35×10^5	$J\,kg^{-1} = m^2\,s^{-2}$
$c_{p,i}$	Specific heat capacity of ice	2009	$J\,kg^{-1}\,K^{-1}$
$c_{p,m}$	Specific heat capacity of water	3974	$J\,kg^{-1}\,K^{-1}$
$\rho_m w_b$	Meltrate of ice		$kg\,m^{-2}\,s^{-1}$

TABLE 2.1: Parameters and variables

where g is the gravitational acceleration and g' is the reduced gravity given by

$$g' = g\frac{|\rho_1 - \rho_2|}{\rho_2}, \tag{2.3}$$

for a two-layer system of water with density ρ_1 in the upper layer and with density ρ_2 in the lower.

C_{2D} and C_{3D} denote the Courant numbers for the 2D and 3D steps, respectively. δt_{2D} is the 2D time step, and δt_{3D} is the 3D time step. For a fixed spatial resolution and fjord depth, δt_{2D} is chosen to keep the C_{2D} below unity. The choice of δt_{3D} is dependent on the stratification of the water column; for areas with water of very low density in the upper layer, the 3D time step must be accordingly small to ensure that the Courant number is kept below unity. If chosen too large, the propagation of internal waves is not resolved, which may result in instabilities.

2.1.2 Melt rate parameterization / thermodynamic model of ice–ocean interaction

There are three physical constraints at the ice–ocean interface: the interface must be at the freezing point, and heat and salt must be conserved during phase changes (Holland and Jenkins, 1999).

2.1.2.1 Ice–ocean boundary temperature and freezing point dependence

The linearized version of the equation for the freezing point of seawater is

$$T_b = \lambda_1 S_b + \lambda_2 + \lambda_3 p_b, \tag{2.4}$$

where λ_{1-3} are empirical constants (Table 2.1) and the subscript b denotes that the temperature T, salinity S and pressure p are at the ice–ocean boundary.

2.1.2.2 Conservation of heat

At the interface between the ice and the ocean, the divergence of heat flux $Q_i^T - Q_m^T$ between the ice and the ocean balances the sink or source of latent heat Q_{lat}^T caused by melting or freezing:

$$Q_i^T - Q_m^T = Q_{lat}^T, \tag{2.5}$$

where the latent heat flux is given by

$$Q_{lat}^T = -\rho_m w_b L_f, \tag{2.6}$$

where $w_b\,[\mathrm{m\,s^{-1}}]$ is the meltrate of the glacier ice so that $\rho_m w_b\,[\mathrm{kg\,m^{-2}\,s^{-1}}]$ represents the mass of ice that is melted per area and time (Holland and Jenkins, 1999).

The rate at which the mixed layer temperature relaxes toward the freezing point is governed by the diffusion of heat through the oceanic boundary layer. The second term in Equation 2.5 has to be expressed by a parameterization due to turbulence in the boundary layer causing a nonlinear temperature profile and a variable diffusivity. This is done by using a thermal exchange velocity turbulent transfer coefficient for temperature, (Sciascia et al., 2013), so that the term is given by

$$Q_m^T = -\rho_m c_{p,m} \gamma_T (T_b - T_m). \tag{2.7}$$

The first term in Equation 2.5 involves the temperature gradient between the ice and the boundary and represents the heat conducted between the sea water and the ice. It may be expressed as

$$Q_i^T = -\rho_i c_{p,i} k (T_i - T_b). \tag{2.8}$$

2.1.2.3 Conservation of salt

A flux of salt from the seawater to the ice–ocean boundary is needed to maintain the boundary salinity in the presence of fresher water from subglacial discharge and submarine melting (Holland and Jenkins, 1999). The freshwater flux associated with melting of the glacier ice is given by

$$Q^S_{brine} = \rho_m w_b (S_i - S_b). \tag{2.9}$$

This flux is balanced by the salt flux divergence at the ice–ocean boundary,

$$Q^S_{brine} = Q^S_i - Q^S_m, \tag{2.10}$$

where Q^S_i is the diffusive flux of salt into the glacier ice, which is identically zero, and Q^S_m is the salt flux from the ocean to the boundary given by

$$Q^S_m = \rho_m \gamma_S (S_m - S_b), \tag{2.11}$$

where γ_S is the haline Stanton number (Section 2.1.2.4; Table 2.1).

2.1.2.4 Turbulence in the ice–ocean boundary layer / turbulent transfer coefficients

The effects of turbulence in the boundary layer between ice and ocean are parameterized by turbulent transfer coefficients $\gamma_{T,S}$.

Earlier, modelling of the thermohaline circulation under ice shelfs has been done with constant values for the transfer coefficients (Hellmer and Olbers, 1989). However, it has been shown that better agreement with measurements of submarine meltrates can be achieved by letting the transfer coefficients have a functional dependency on water velocities (Holland and Jenkins, 1999; Jenkins et al., 2010). Holland and Jenkins (1999) also argues it is more realistic to let them vary with the friction velocity since it is a result of turbulence in the mixed layer. Sensitivity analysis by Sciascia et al. (2013) on the velocity dependency of the transfer coefficients suggests that the vertical velocity near the glacier front has a leading order impact on the submarine meltrate and especially its vertical structure. Therefore, in this study, the turbulence in the ice–ocean boundary layer is parameterized using transfer coefficients which are dependent on the water velocity near the glacier front. They are given by

$$\gamma_{T,S} = \sqrt{C_d}\, \Gamma_{T,S}\, U_b, \tag{2.12}$$

where $\sqrt{C_d}\,\Gamma_T$ and $\sqrt{C_d}\,\Gamma_S$ is the thermal and haline Stanton number, respectively (Table 2.1) and $U_b = \sqrt{u_b^2 + w_b^2}$ is the magnitude of the velocity at the ice–ocean boundary, assumed to be determined mainly by the vertical velocity component of the buoyant plume by the glacier front (the horizontal component induced by entrainment is much smaller) (Sciascia et al., 2013).

2.2 Model setup

A simple two-dimensional setup of the non-hydrostatic model is chosen. The glacier front is vertical and grounded at the bottom, and the bottom is flat, which makes the vertical resolution uniform. There is no tidal forcing nor wind forcing on the water column in the simulations. The surface is free, and at the open boundary, there is a 50 m thick sponge layer restoring the temperature and salinity conditions of the open ocean to those prescribed as initial conditions. This is done with a flow relaxation scheme (FRS) in which the variable ϕ gets updated after each model time step by

$$\phi = (1 - \alpha)\phi_M + \alpha\phi_F, \tag{2.13}$$

where ϕ_M is the unrelaxed value computed by the model, ϕ_F is the specified boundary value equal to the intial condition in the sponge layer, and α varies from 1 at the model boundary to 0 at the end of the layer towards the interior of the fjord (Berntsen, 2000).

The model width is one grid cell of size $\delta y = 10\,\mathrm{m}$. The along-fjord spatial resolution is uniform with a grid size of $\delta x = 10\,\mathrm{m}$. The timesteps are $\delta t_{3D} = 1.2\,\mathrm{s}$ and $\delta t_{2D} = 0.08\,\mathrm{s}$, which satisfy the CFL-criteria (Section 2.1.1).

2.2.1 Subglacial discharge

For the Sermilik Fjord simulations, the subglacial discharge ranges between $0.29\,\mathrm{m^3\,s^{-1}}$ and $8.70\,\mathrm{m^3\,s^{-1}}$, as in Sciascia et al. (2013). These fluxes are obtained by scaling the estimated total summer surface runoff of $174\,\mathrm{m^3\,s^{-1}}$ based on how this volume of surface meltwater gets discharged into the fjord. As the number and size of the drainage channels are unknown, one may consider two possibilities which provide plausible lower and upper bounds of the rescaled flux of subglacial discharge in the simulations. The lower bound of $0.29\,\mathrm{m^3\,s^{-1}}$ is obtained by assuming that the summer runoff of $174\,\mathrm{m^3\,s^{-1}}$ is uniformly discharged along the base of the Helheim Glacier. Using a width of 6 km as in Sciascia et al. (2013), the lower bound is a flux per unit width of $0.029\,\mathrm{m^2\,s^{-1}}$, which when rescaled to the model width of 10 m becomes $0.29\,\mathrm{m^3\,s^{-1}}$. If, on the other hand, the

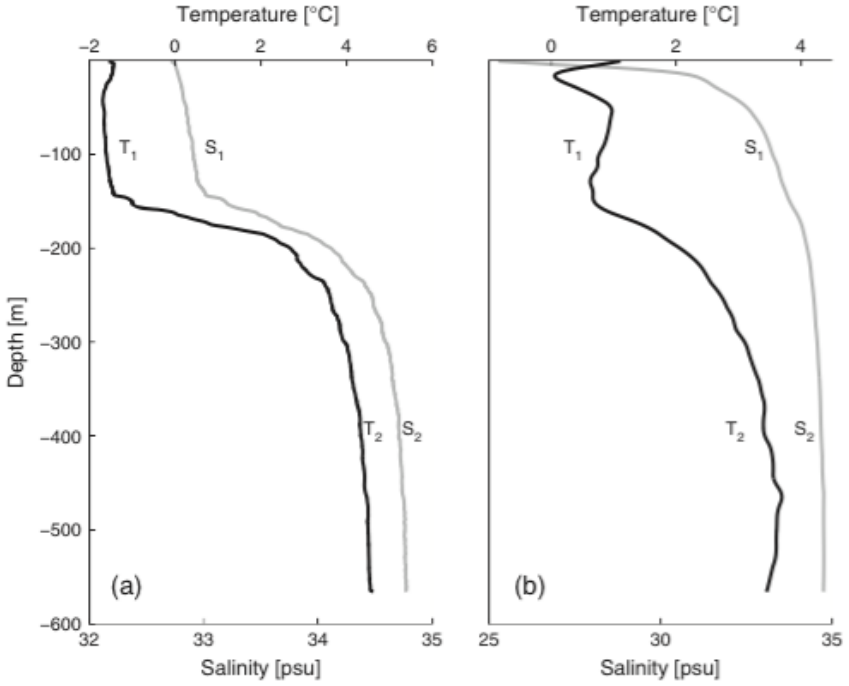

FIGURE 2.1: Vertical profiles of temperature (black curves) and salinity (gray curves) mid-fjords in Sermilik Fjord obtained by Straneo et al. (2011). Measurements were taken in March 2010 (left) and August 2009 (right). The figure is made by Sciascia et al. (2013).

total flux of $174\,\mathrm{m^3\,s^{-1}}$ is discharged through a single channel which is 200 m wide (assuming that there are no other drainage channels along the glacier base), the upper bound is $0.87\,\mathrm{m^2\,s^{-1}}$ which is $8.7\,\mathrm{m^3\,s^{-1}}$ when rescaled to the 10 m wide model channel.

The subglacial discharge enters the fjord at the bottom as a river of freshwater with a temperature determined by the freezing point at that pressure. The velocity of the water is determined by the volume flux and the size of the meltwater channel, i.e.,

$$u_{Q_{sg}} = \frac{Q_{sg}}{A}. \tag{2.14}$$

$A = 200\,\mathrm{m^2}$ is the area of the meltwater channel out from which glacial meltwater flow. The meltwater channel occupies two vertical model cells of 10 m height each and 10 m width.

2.2.2 Initial conditions

Generally, the model is initialized with an idealized stratification of two layers; a lower thick layer of relatively warm and saline water of Atlantic origin in the warm years or saline and locally cooled water in the cold years capped by a thinner layer of fresher and

colder water (Table 2.2), based on the observed two-layer stratification in the Sermilik Fjord (Figure 2.1, left panel). The fjord depth is 600 m in the Sermilik Fjord simulations.

2.2.3 Submarine meltrate

For each model time step, the submarine meltrate is calculated from the equations for the thermodynamic model of the ice–ocean interaction (Section 2.1.2) and rescaled to get the units of $\mathrm{m\,yr^{-1}}$.

The submarine meltrate at a given depth z is $smr(z)$. Its maximum value smr_{max} refers to the maximum with respect to depth, and its vertically averaged value is given by

$$\overline{smr} = \frac{1}{H_t} \int_{-H_t}^{0} smr(z)\,\mathrm{d}z, \tag{2.15}$$

where H_t is the depth of the fjord.

2.3 Model experiments

A series of experiments are conducted with the aim of studying the glacier-driven circulation and submarine melting in absence of external forcings such as tides, wind stress and rotational dynamics. It has been shown that glacial fjords are to a great extent forced by exchanges of water masses with the shelf region outside the fjords, and this is reflected in the water masses present in the fjord as the model is initialized.

First, we repeat a selection of the simulations of the glacier-driven fjord dynamics in the Sermilik Fjord performed by Sciascia et al. (2013) and try to reproduce their results. Then we study the submarine melting of a glacier front in a fjord in which the water properties, stratification and depth are varied.

2.3.1 Reproduction of idealized simulations of the Sermilik Fjord

Control experiment – WIN. The control experiment is initialized in a two-layer setup with winter water properties (Figure 2.1, left panel) and with a subglacial discharge of $Q_{sg} = 0.01\,\mathrm{m^3\,s^{-1}}$ in order to initialize the circulation and submarine melting which requires an initial velocity in the cells adjacent to the glacier front.

	Q_{sg} [$m^3 s^{-1}$]	T_{PW} [°C]	T_{AW} [°C]	S_{PW}	S_{AW}	H_{PW} [m]	H_{AW} [m]
WIN	0.01	−1.5	4.0	32.9	34.6	150	450
SUM	4.3	−1.5	4.0	32.9	34.6	150	450
SUMD	0.01 to 8.7	−1.5	4.0	32.9	34.6	150	450
TEMP	0.01	−1.5	−0.36 to 8.0	32.9	34.6	150	450
TEMPS	4.3	−1.5	0.0 to 8.0	32.9	34.6	150	450
SUMD2	0.01 to 8.7	−1.5	2, 4, 6	32.9	34.6	150	450
DEPTH	0.01, 4.3	−1.5	4.0	32.9	34.6	50	150
PWT	0.01, 4.3	−1.5	4.0	32.9	34.6	150	50

TABLE 2.2: Description of the setup used in each (series of) simulation(s). (More detailed explanation in Section 2.3.)

Summer experiment – SUM. In the summer experiment, the effect of subglacial discharge is studied. The experiment is identical to *WIN* but with a steady subglacial discharge of $Q_{sg} = 4.30\,m^3\,s^{-1}$, which corresponds to a situation where the estimated summer surface runoff of $Q_{tot} = 174\,m^3\,s^{-1}$ is channeled through a 400 m wide opening.

Sensitivity to subglacial discharge – SUMD.
With the water properties as in *WIN*, the influence of the flux of subglacial discharge on submarine melting and fjord dynamics is studied. Due to the highly variable subglacial discharge in summer, its flux is varied in the range $0.29\,m^3\,s^{-1}$ to $8.70\,m^3\,s^{-1}$ (Section 2.2.1). In addition, simulations with Q_{sg} in the range $0.01\,m^3\,s^{-1}$ to $0.29\,m^3\,s^{-1}$ are performed for continuity and for studying the sensitivity for fluxes close to zero.

Sensitivity to AW temperature – TEMP and TEMPS.
The temperature of the AW layer is varied over a plausible range. In *TEMP*, T_{AW} is varied with 1 °C increments from 0 °C to 8 °C, and, in addition, one simulation is done with $T_{AW} = -0.36$ °C, the temperature of the freshwater discharged at depth. In *TEMPS*, T_{AW} is varied with 2 °C increments from 0 °C to 8 °C.

2.3.2 Further studies

Sensitivity to subglacial discharge for various AW temperatures – SUMD2 In these simulations, we explore more in depth the influence of the subglacial discharge variability and the AW temperature on the submarine melting to further establish in which ranges of Q_{sg} and T_{AW} changes of these have the greatest influence of the magnitude and the vertical structure of the submarine meltrate.

Depth experiment – DEPTH. We study how the submarine meltrate and plume dynamics respond to a change in the fjord depth by repeating some simulations in a shallow fjord (200 m) and test the hypothesis of whether a smaller depth will inhibit the plume acceleration and thus limit the submarine melting. The variation of fjord depth is partly motivated by studying whether the plume dynamics is significantly different at glacier fronts in the end of shallower fjord, for instance fjords in Spitsbergen. Also, when the glacier front melts at a high rate in a deep fjord, the front retreat to a position further infjords where it is likely the depth is smaller.

Sensitivity to PW thickness in a shallow fjord – PWT. In these simulations, we explore the fjord circulation in two scenarios – one in which the upper PW layer is 150 m thick, as in the Sermilik simulations„ and one in which the ratio of the thicknesses of the PW layer and the AW layer is the same as in the Sermilik runs, i.e. a 50 m PW capping 150 m of AW. In both cases, a winter and a summer simulation is done.

2.4 Data analysis / statistics

The model function has the form $f(x, \beta)$ where β contains parameters which are adjusted so that the model fits the data set $(x_i, y_i), i \in \{1, ..., n\}$ in the least square sense, which occurs when the sum of squared residuals

$$SS_{res}(\beta) = \sum_{i=1}^{n} r_i^2(\beta) = \sum_{i=1}^{n} (y_i - f(x_i, \beta))^2 \tag{2.16}$$

is minimal.

We apply the method of least squares in terms of linear estimation (linear in the parameters in β).

$SS_{res}(\beta)$ is the total variance that is not explained (accounted for) by the linear regression model given by

$$y_i = f(x_i, \beta) + r_i \tag{2.17}$$

and

$$f(x_i, \beta) = \beta_0 + \beta_1 x_i. \tag{2.18}$$

2.4.1 Goodness of fit

The correlation/coefficient of determination R^2 is a measure of the goodness of fit of the regression curves and can be expressed in several ways.

Generally it is defined as a function of the sum of squared residuals,

$$R^2 = 1 - \frac{SS_{res}}{SS_{tot}}, \tag{2.19}$$

but given that

$$SS_{res} = SS_{tot} - SS_{reg}, \tag{2.20}$$

where

$$SS_{tot} = \sum_{i=1}^{n} (y_i - \overline{y})^2 \tag{2.21}$$

is the variance in the data (proportional to the sample variance), and

$$SS_{reg} = \sum_{i=1}^{n} (f(x_i, \beta) - \overline{y})^2 \tag{2.22}$$

expresses the variance of the values predicted by the model (i.e., the explained variance), the coefficient of determination can be expressed as

$$R^2 = \frac{SS_{reg}}{SS_{tot}}, \tag{2.23}$$

which shows that the coefficient of determination is a measure of how much of the total variance is explained by the regression model.

Chapter 3

Results

3.1 Reproduction of 2D runs in Sermilik, Greenland

3.1.1 Control experiment – WIN

The control experiment is initialized with winter water properties and with a minor subglacial discharge of $Q_{sg} = 0.01\,\mathrm{m^3\,s^{-1}}$ (Section 2.3.1).

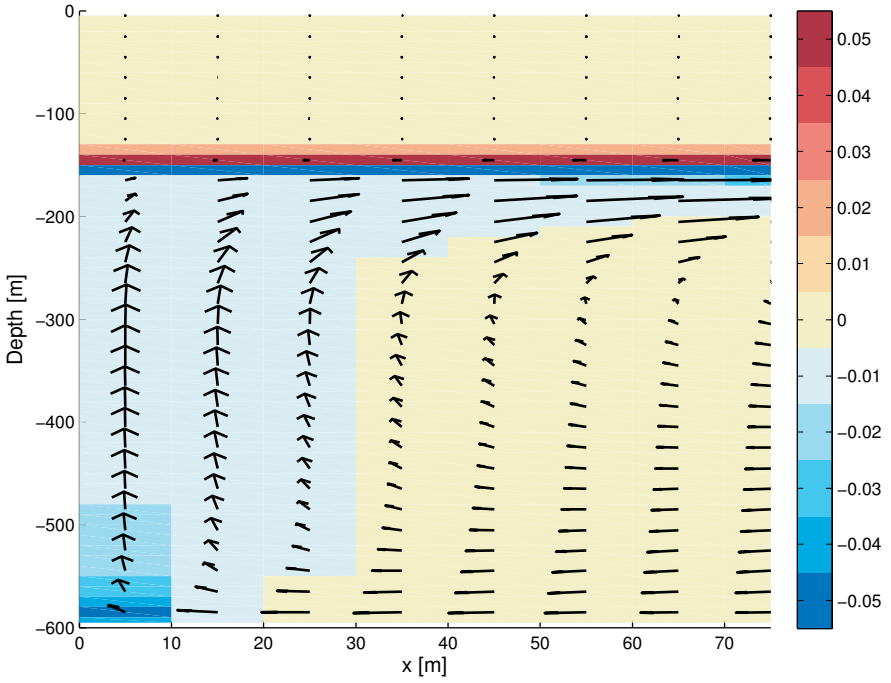

FIGURE 3.1: Control experiment *WIN*. Current vectors (x, z) overlaid the salinity anomaly (initial salinity field subtracted from the temporally averaged salinity field). Red (blue) colour represent more (less) saline water than initially. The glacier front is to the left.

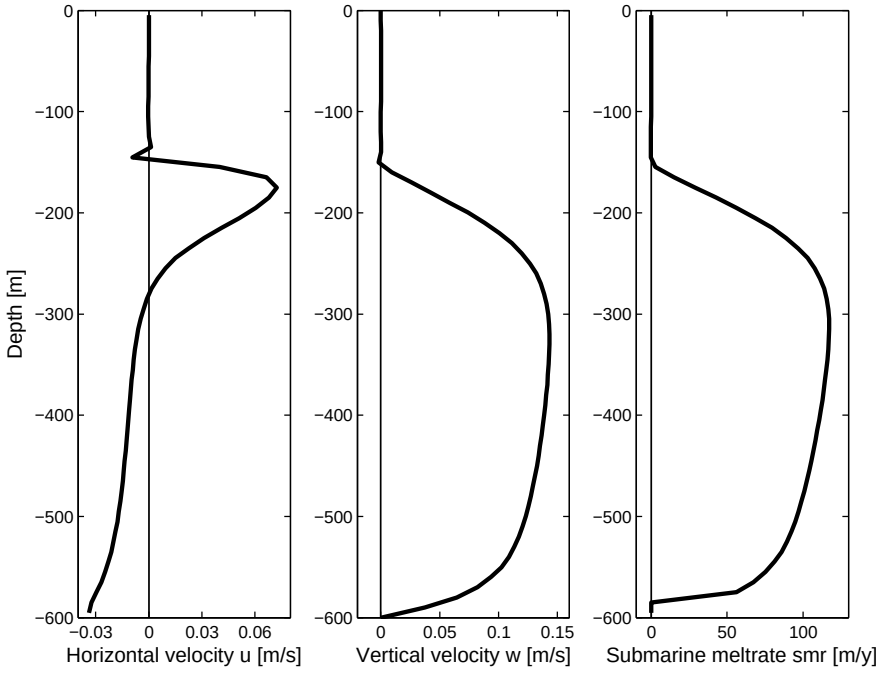

FIGURE 3.2: Control experiment *WIN*. Vertical profiles of (left) horizontal velocity $u\,[\mathrm{m\,s^{-1}}]$ representing an average over the 100 m (10 grid cells) closest to the glacier front, (middle) vertical velocity $w\,[\mathrm{m\,s^{-1}}]$ in the 10 m by the glacier front, and (right) submarine meltrate $smr\,[\mathrm{m\,yr^{-1}}]$.

Submarine melting at the glacier terminus leads to a buoyant plume to form and rise along the glacier front. In the model, the melting decreases the salinity of the fjord water close to the ice; this corresponds to fresh subglacial discharge and glacial meltwater entraining the ambient saline fjord water. This gives rise to a relatively fresh plume which, due to its low density, ascends close to the glacier front until it reaches its neutral density level – the depth at which the plume density matches the density of the ambient water so that the plume no longer is buoyant. At this depth, the plume water containing meltwater from the glacier front, subglacial discharge, and entrained fjord water flows horizontally away from the glacier front. This circulation is shown Figure 3.1.

After a few hours, the fjord circulation and submarine melting have reached an almost steady state in which there is no major variations in the neither the magnitudes of the currents and meltrate nor their vertical structure. In the following, plume velocity refers to the water velocity in the plume, mostly in the model cells next to the glacier front, and plume acceleration refers to the vertical change of the vertical plume speed.

Within the 50 m above the bottom, the plume accelerates upwards to $0.1\,\mathrm{m\,s^{-1}}$; further away from the bottom, the acceleration (with respect to z) is smaller, and the plume reaches its maximum vertical velocity of $w = 0.14\,\mathrm{m\,s^{-1}}$ at 350 m depth. From this maximum, the vertical velocity along the glacier front decreases to zero at the interface between the AW layer and the PW layer (Figure 3.2, middle panel). This is because the

	Q_{sg} [$\mathrm{m^3\,s^{-1}}$]	T_{AW} [°C]	$\overline{smr}$ [$\mathrm{m\,yr^{-1}}$]
WIN	0.01	4.0	67.1
SUM	4.30	4.0	769.0
SUMD	0.29 to 8.70	4.0	287.5 – 930.9
TEMP	0.01	−0.36 to 8.0	42.9 – 77.3
TEMPS	4.30	0.0 to 8.0	488.0 – 1043

TABLE 3.1: Dependency of subglacial discharge and temperature on submarine meltrate.

density of the plume is between that of the PW and the AW, and the vertical velocity of the plume is not sufficient to penetrate through the interface. Consequentely, the glacially modified water in the plume continues horizontally along the interface. Due to conservation of volume, this interfacial outflow drives a return current at depth. The return current transports fjord water towards the glacier front at depths between 300 m and 600 m at an average speed of $0.02\,\mathrm{m\,s^{-1}}$ in the 100 m closest to the glacier (Figure 3.2, left panel).

The strongest current away from the glacier front, in the thin layer below the pycnocline, is about $0.08\,\mathrm{m\,s^{-1}}$, that is, about 7 km per day. With this speed throughout the simulation period of 20 days, the signal would not reach the open ocean boundary; however, due to generation of artificial currents close to the FRS zone by the open ocean boundary, temporal averaging of the variables is done over a time period in which there are no impacts of the artificial currents introduced by the open model boundary on the results.

The submarine meltrate $smr(z)$ is to a great extent dependent on the vertical velocity of the plume $w(z)$ (Figure 3.2), evident from the shape of the profiles of w and smr. A faster plume melts locally more ice since the entrainment of ambient (warm) water increases with the vertical velocity by the glacier front. Thus, the inclusion of velocity-dependent turbulent transfer coefficients $\gamma_{T,S}$ in the meltrate parameterization of the ice–ocean boundary induce this strong dependency of smr on w.

The vertically averaged submarine meltrate for the *WIN* simulation is $\overline{smr} = 67.1\,\mathrm{m\,yr^{-1}}$, which is in good agreement with the corresponding simulation of Sciascia et al. (2013) ($70\,\mathrm{m\,yr^{-1}}$).

3.1.2 Summer experiment – SUM

This simulation is initialized in the same two-layer setup with winter water properties as in the control experiment *WIN*, but with a steady subglacial discharge of $4.3\,\mathrm{m^3\,s^{-1}}$

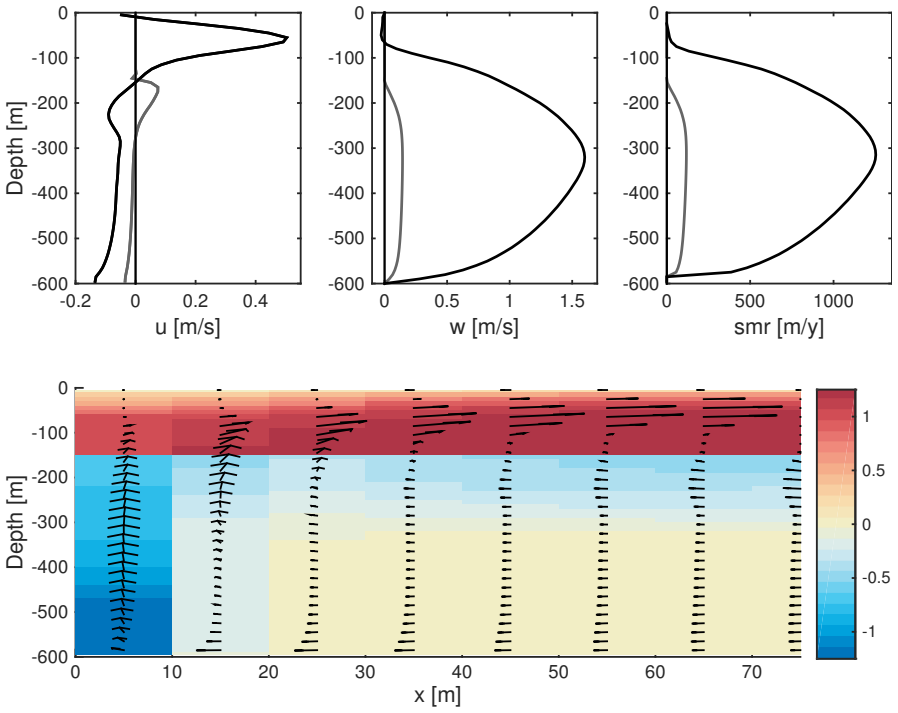

FIGURE 3.3: Summer experiment *SUM*. Vertical profiles of (upper left) horizontal velocity $u\,[\mathrm{m\,s^{-1}}]$ averaged over the 100 m by the glacier front, (upper middle) vertical velocity $w\,[\mathrm{m\,s^{-1}}]$ in the 10 m by the glacier front, and (upper right) submarine meltrate $smr\,[\mathrm{m\,yr^{-1}}]$. Black curves are profiles for the *SUMD* simulation; gray curves are profiles for the *WIN* simulation (3.1.1) for comparison. Lower panel: Current vectors (x, z) overlaid the salinity anomaly (initial salinity field subtracted from the temporally averaged salinity field). Red (blue) colour represent more (less) saline water than initially. The glacier front is to the left.

(Section 2.3.1, Table 2.2) to study the effect of surface meltwater being discharged into the fjord at depth. The value of Q_{sg} is obtained by assuming that the estimated summer surface runoff is channeled through a 400 m wide opening and rescaled to be representable to the vertical slice in the model (Section 2.2.1).

The subglacial discharge provides an additional forcing on the plume. The velocity with which the subglacial discharge enters the fjord at depth is about $0.02\,\mathrm{m\,s^{-1}}$ (Equation 2.14), which is less than 2 % of the mean plume speed next to the glacier front in the AW layer but nevertheless contributes to the high vertical plume speed by increasing the meltrate of the glacier ice and thus increasing the plume buoyancy due to the entrained meltwater. The vertically averaged vertical plume speed in the water column by the glacier front is an order of magnitude larger than in the control simulation (Figure 3.3, upper middle panel). Also in this simulation, the submarine melting is highly dependent on the plume speed, so the vertically averaged meltrate $\overline{smr}$ of $769.0\,\mathrm{m\,yr^{-1}}$ in summer is more than ten times higher than that in winter (Figure 3.3, upper right panel). This meltrate is also in agreement with that obtained by Sciascia et al. (2013) of $738\,\mathrm{m\,yr^{-1}}$.

The increased plume speed by the glacier front and increased in summer compared to winter leads to a quicker horizontal outflow of a larger volume of glacially modified waters (Figure 3.3, upper left panel). The core of the outflow current reaches a speed over $0.4\,\mathrm{m\,s^{-1}}$ and is elevated compared to the winter season outflow current. The outflow occurs closer to the surface since the large addition of meltwater from the glacier front lincreases the plume volume and speed so that the water has sufficient momentum to penetrate through the interface between the PW layer and the AW layer, causing higher salinity anomalies around the interface (Figure 3.3, lower panel) and more mixing across the interface.

3.1.3 Influence of variable subglacial discharge - SUMd

In these simulations, the impacts of a varying subglacial discharge on the submarine melt rate and on the plume dynamics are studied. For each simulation, the subglacial discharge value Q_{sg} is constant, and in the series of simulations, Q_{sg} is varied over the range $0.01\,\mathrm{m^3\,s^{-1}}$ to $8.70\,\mathrm{m^3\,s^{-1}}$ (Sections 2.3.1 and 2.2.1, Table 2.2).

With increasing subglacial discharge, the submarine melting increases and the fjord circulation near the glacier front becomes faster and more turbulent, with overall higher current velocities and more oscillations at the layers' interface.

The plume is forced by two water masses of glacial origin: the subglacial discharge whose flux we vary in this experiment, and the meltwater from the submarine melting of the glacier front. As the subglacial discharge increases, the submarine meltrate increases due to the larger plume velocity which causes a larger rate of turbulent mixing of heat between the ocean and the ice front. As the increased plume velocity leads to more melting at the glacier front, the larger amount of meltwater from the submarine melting gets entrained into the plume, makes it more buoyant and therefore contributes to the larger vertical plume speed.

3.1.3.1 Vertically integrated smr as function of subglacial discharge

In the case with the lowest summer freshwater flux, $Q_{sg} = 0.29\,\mathrm{m^3\,s^{-1}}$, the vertically averaged meltrate $\overline{smr} = 287.5\,\mathrm{m\,yr^{-1}}$ is 223.8 % larger than the winter meltrate and also larger than the meltrate found by Sciascia et al. (2013).

With Q_{sg} equal to the upper bound of the summer freshwater flux of $0.29\,\mathrm{m^3\,s^{-1}}$, $\overline{smr} = 930.9\,\mathrm{m\,yr^{-1}}$ is in fairly good agreement with the result of Sciascia et al. (2013) of $\overline{smr} = 1111\,\mathrm{m\,yr^{-1}}$.

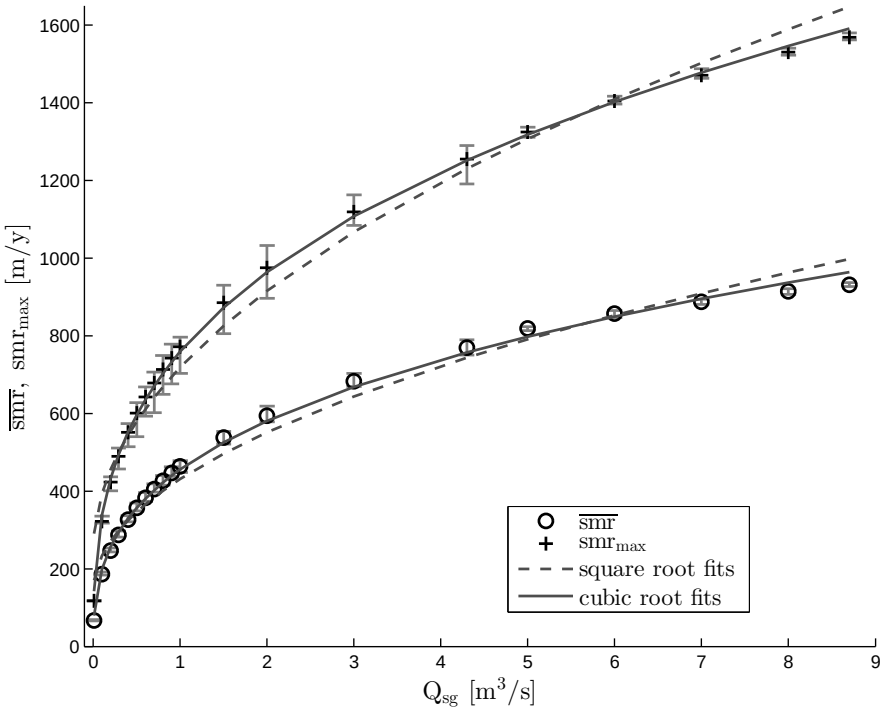

FIGURE 3.4: Sensitivity to subglacial discharge (*SUMD*). $\overline{smr}$ (vertically averaged values, black circles) and smr_{max} (black plus signs) as a function of Q_{sg}. Solid curves indicate the cubic root fits, and dashed curves indicate the square root fits.

Over the range $0.01\,\mathrm{m^3\,s^{-1}}$ to $8.70\,\mathrm{m^3\,s^{-1}}$, $\overline{smr}$ increases with the cubic root of Q_{sg} (Figure 3.4).

3.1.3.2 Salinity distribution and fjord circulation for various subglacial discharge fluxes

The dynamics at the glacier front depend on the magnitude of the subglacial discharge and goes through three regimes which were described by Sciascia et al. (2013). For small subglacial discharge fluxes – an example is the control simulation (Figure 3.1) – the circulation and submarine melting mostly takes place in the AW layer, leaving the PW layer close to motionless. These are characteristics of the regime I circulation. Increasing the subglacial discharge, the fjord enters regime II in which the plume becomes quicker, larger and more buoyant due to the increasing submarine melting. Therefore it overshoots the interface between the layers, and due to the low density of the PW layer relative to the plume density, the plume descends into the AW layer where it is buoyant, and establishes an oscillation at the interface. Glacially modified water gets transported away from the glacier front along this interfacial wave. Regime II has a large degree of mixing between the PW layer and the AW layer due to the large-amplitude oscillations. Regime III, which occurs for even larger subglacial discharge fluxes, is characterized by

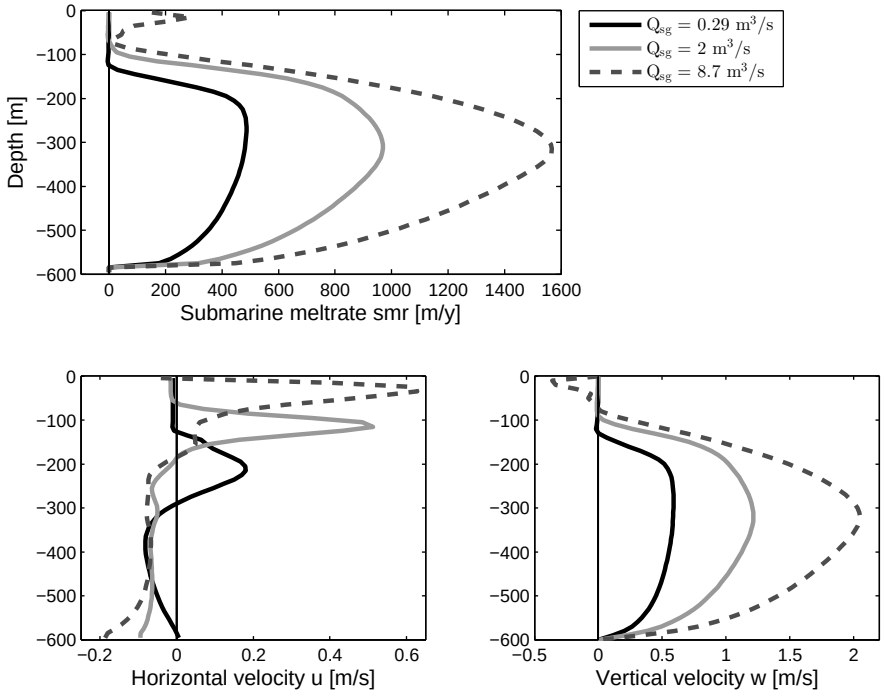

FIGURE 3.5: Sensitivity to subglacial discharge (*SUMD*). Upper panel: profiles for submarine meltrate [$\mathrm{m\,yr^{-1}}$]. Lower panel, left: horizontal velocity [$\mathrm{m\,s^{-1}}$] averaged over the 100 m closest to the glacier front. Lower panel, right: vertical velocity [$\mathrm{m\,s^{-1}}$] at the glacier front. All profiles have been averaged over a steady state period of 120 hours. Solid black (dashed dark-gray) lines are profiles for the lower (upper) limit of $0.29\,\mathrm{m^3\,s^{-1}}$ ($8.7\,\mathrm{m^3\,s^{-1}}$) for the Sermilik fjord, representative for regime I (III), and the solid light-gray lines are profiles for $Q_{sg} = 2.0\,\mathrm{m^3\,yr^{-1}}$ representative for regime II (Section 3.1.3.2).

a surface outflow of glacially modified water. In this regime, the plume has a buoyancy sufficiently large to penetrate through the interface, ascend through the PW layer and establish an outflow at surface level. Examples of the various circulation patterns are shown in Figure 3.6.

Increasing the subglacial discharge an order of magnitude, i.e., from $0.01\,\mathrm{m^3\,s^{-1}}$ in the *WIN* control simulation to $0.10\,\mathrm{m^3\,s^{-1}}$, the salinity distribution and current pattern change in the upper part of the AW layer. The main features of the regime I flow as in *WIN* is kept for the lower range of subglacial discharge in the *SUMD* simulations, but already for $Q_{sg} = 0.10\,\mathrm{m^3\,s^{-1}}$ a wave pattern in the salinity anomaly and outflow develop in the upper part of the AW layer. As Q_{sg} increases further up to the summer lower bound of $0.29\,\mathrm{m^3\,s^{-1}}$, the amplitude of the wave in the upper part of the AW layer increases. However, for these Q_{sg} values there is no significant overshooting of the interface and the circulation resembles to a rather large extent that of the *WIN* control run with a $0.01\,\mathrm{m^3\,s^{-1}}$ flux.

For $Q_{sg} \leq 1.50\,\mathrm{m^3\,s^{-1}}$, the outflow in the vicinity of the glacier front is in a 200 m thick layer near the interface. The u maxima increase from $0.1\,\mathrm{m\,s^{-1}}$ to $0.2\,\mathrm{m\,s^{-1}}$ when Q_{sg}

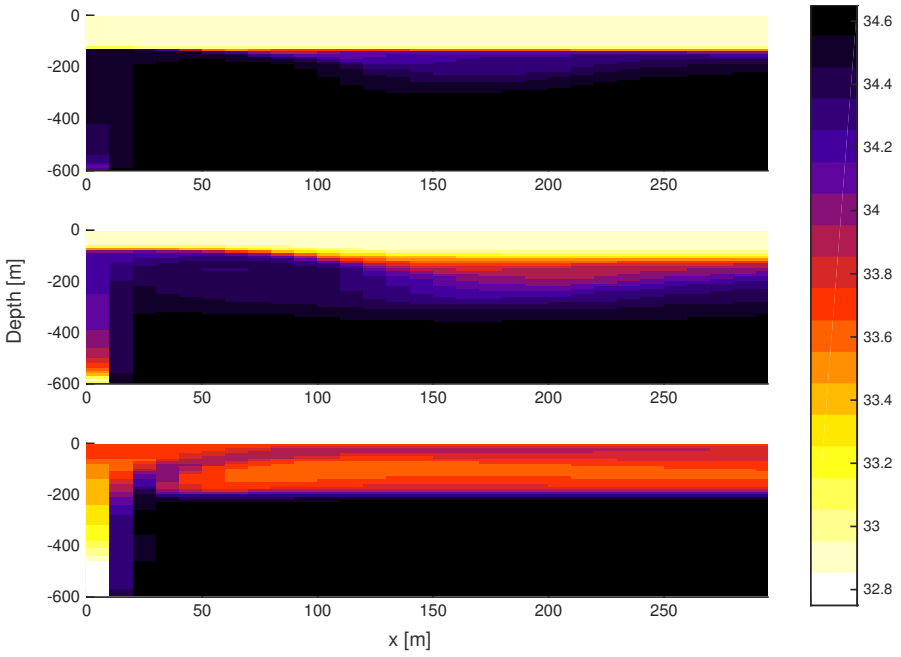

FIGURE 3.6: Sensitivity to subglacial discharge (*SUMD*). Salinity distribution in the 300 m closest to the glacier front. Upper panel: $Q_{sg} = 0.29\,\mathrm{m^3\,s^{-1}}$ (lower bound on the summer discharge), regime I flow. Middle panel: $Q_{sg} = 2.0\,\mathrm{m^3\,s^{-1}}$, regime II flow. Lower panel: $Q_{sg} = 8.7\,\mathrm{m^3\,s^{-1}}$ (upper bound on the summer discharge), regime III flow.

vary in the range $0.1\,\mathrm{m^3\,s^{-1}}$ to $1.5\,\mathrm{m^3\,s^{-1}}$. For $1.50\,\mathrm{m^3\,s^{-1}}$ and higher, the fjord adapts to a regime II circulation as a higher vertical velocity along the glacier front develops, causing it to overshoot the interface between the PW layer and the AW layer and thereby gain momentum (due to its high density relative to the PW density) to descend farther into the AW layer and make the interfacial oscillations larger, leading to wave troughs occasionally breaking off.

The intermediate values for subglacial discharge of $2.0\,\mathrm{m^3\,s^{-1}}$ to $4.3\,\mathrm{m^3\,s^{-1}}$ mark a transition for the flow dynamics at the glacier front. The mean profile of horizontal velocity in the vicinity of the glacier front changes significantly within this Q_{sg} range; with increasing Q_{sg}, the depth of the outflow of glacially modified water changes from being about 50 m below the initial interface to ending up in the middle of the PW layer (Figure 3.5) or quite close to the surface. The flow for this Q_{sg} is still within regime II as the outflow occurs at the layers' interface further away from the glacier front. Due to the rather large plume velocity and the large overshooting of the interface, melting and entrainment of meltwater also takes place in the PW layer, but the plume nevertheless has a density just too high to fully penetrate through the PW layer and reach the surface.

For subglacial discharge fluxes of $5.0\,\mathrm{m^3\,s^{-1}}$ and larger, the main outflow of glacially modified water occurs in the upper part of the PW layer (Figure 3.5, dashed line), meaning the fjord circulation is of the regime III type. The strength of the current core,

averaged over 100 m closest to the glacier front, is roughly $0.5\,\mathrm{m\,s^{-1}}$ to $0.6\,\mathrm{m\,s^{-1}}$. The outflow velocity decreases towards the interface and is about $0.1\,\mathrm{m\,s^{-1}}$ in the lower half of the PW layer and near the interface. The return current of $0.1\,\mathrm{m\,s^{-1}}$ in the AW layer is nearly vertically uniform (Figure 3.5), with the exception of an increase in the lower 100 m. 1 km away from the glacier front, the circulation is more horizontal; the surface outflow is rather strong, with a maximum of $1\,\mathrm{m\,s^{-1}}$ occuring right below the surface. In contrast to the circulation close to the glacier front, 1 km from the front, there is also a weak return flow within the PW layer and an even weaker outflow ($2\,\mathrm{cm\,s^{-1}}$ to $5\,\mathrm{cm\,s^{-1}}$) close to the interface. Since the outflow occurs at the surface for the highest values in the Q_{sg} range, there are no oscillations at the interface and therefore less mixing across the interface once the surface outflow has been established.

3.1.4 Influences of changes in Atlantic water temperature – TEMP and TEMPs)

In the *TEMP(s)* simulations, the impact of AW temperature T_{AW} on submarine melting and fjord circulation is studied. Keeping the winter season subglacial discharge value of $Q_{sg} = 0.01\,\mathrm{m^3\,s^{-1}}$ constant, the temperature in the AW layer is varied linearly between $-0.36\,^\circ\mathrm{C}$, $0\,^\circ\mathrm{C}$ and $8\,^\circ\mathrm{C}$ with $1\,^\circ\mathrm{C}$ increments. This corresponds to the likely variability of the deep water (AW) on the shelf outsude the fjord.

The vertically integrated submarine meltrate $\overline{smr}$ increases with increasing AW temperature in both winter and summer (Figure 3.7). The dependency of $\overline{smr}$ on T_{AW} in the studied range is close to linear, which is consistent with the similar MITgcm simulations of Sciascia et al. (2013).

3.1.4.1 Fjord dynamics and submarine melting in winter

Higher temperature in the AW layer leads to less dense water. This causes the density difference between the plume and the ambient water to be smaller, and therefore the plume will ascend more slowly (Figure 3.8, second panel). The effect of changes in temperature on density is not large in saline and cold water but increases with increasing temperature even within the explored temperature range.

Another effect on the varying AW temperature is the stability of the water column. Increasing T_{AW} results in a weakening of the stratification. For $T_{AW} = 8\,^\circ\mathrm{C}$, the weak pycnocline makes the water column susceptible to large vertical motion as the stability is marginal. When the plume reaches the interface, currents at the pycnocline bring colder, fresher water from the PW layer, which gets entrained into the AW layer. The weak

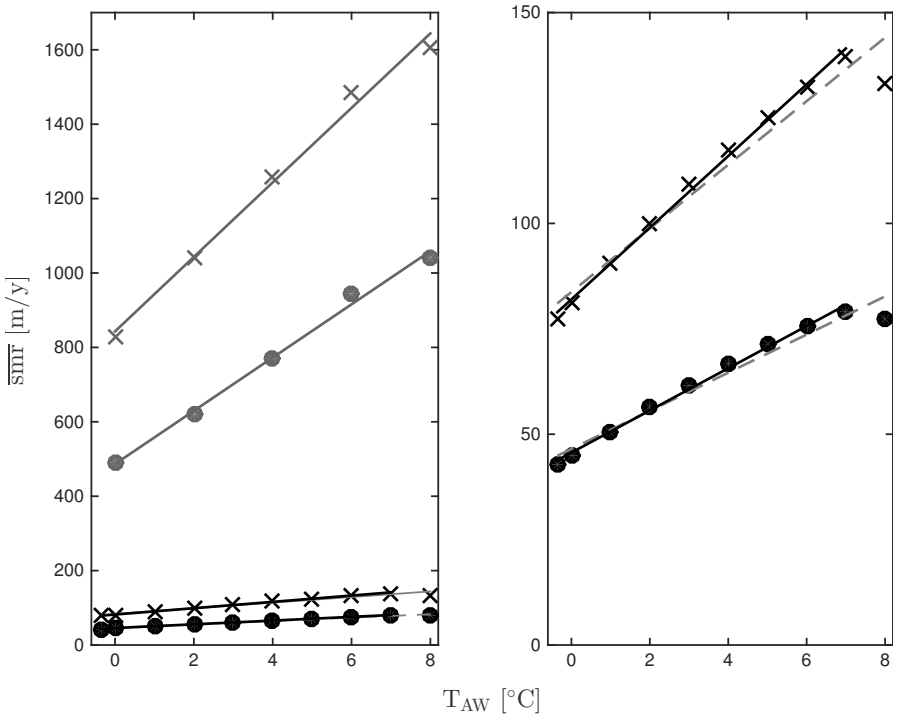

FIGURE 3.7: Vertically averaged submarine meltrate $\overline{smr}$ (circles) and maximum submarine meltrate smr_{max} (crosses) as function of temperature in the AW layer T_{AW}. Solid lines are linear fits. Left panel: Black (gray) symbols denote simulations in *TEMP* (*TEMPs*) without (with) subglacial discharge. Right panel: Only *TEMP*. Dashed lines are linear fits with all values included; solid lines are linear fits with $T_{AW} = 8\,°\mathrm{C}$ excluded.

stability throughout the depth enables quicker vertical mixing. The resulting cooler AW water in the vicinity of the glacier front and more complex circulation in the AW layer cause the submarine meltrate to be smaller for $T_{AW} = 8\,°\mathrm{C}$ than for $T_{AW} = 7\,°\mathrm{C}$ (Figure 3.7).

In the winter simulations *TEMP*, the fjord circulation is of the regime I as in the control simulation (Section 3.1.1). For all AW temperatures, a plume ascends along the glacier front, melts glacier ice and entrains the meltwater, slightly increasing its vertical speed as it ascends. Due to the effect temperature changes have on water density, higher AW temperature leads to a slower plume during winter when the meltwater plume has generally low speed. The change in vertical plume velocity is largest at the depths where w reaches its maximum value, approximately 100 m below the pycnocline (Figure 3.8, second panel). Although the plume flow becomes slower for higher ambient water temperature, the submarine meltrate is larger. Regardless of the AW temperature, the fjord circulation remains in regime I in which the outflow of glacially modified waters is situated in a 100 m thick region below the layers' interface. The outflow speed is about $0.1\,\mathrm{m\,s^{-1}}$ (Figure 3.8, third and fourth panels).

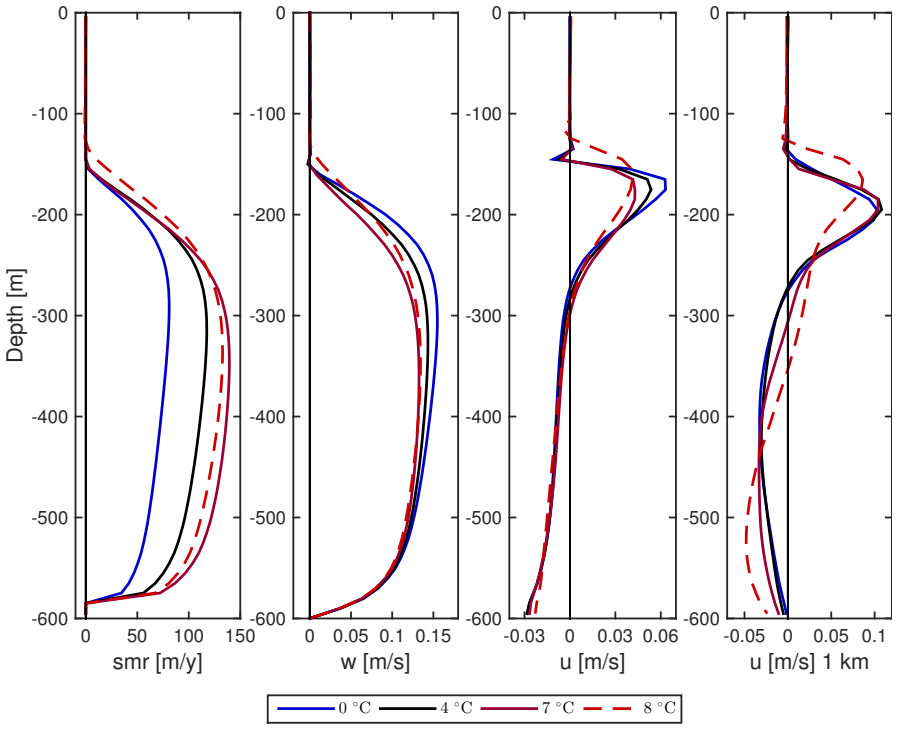

FIGURE 3.8: The effect of variation of AW temperature (−0.36 °C to 8 °C) in winter (*TEMP*). Vertical profiles of (first) submarine meltrate $smr\,[\mathrm{m\,yr^{-1}}]$, (second) vertical velocity $w\,[\mathrm{m\,s^{-1}}]$ in the 10 m closest to the glacier front, (third) horizontal velocity $u\,[\mathrm{m\,s^{-1}}]$ averaged over the 100 m by the glacier front, and (fourth) $u\,[\mathrm{m\,s^{-1}}]$ 1 km away from the front. Profiles for temperatures 0 °C, 4 °C, 7 °C, and 8 °C are shown.

3.1.4.2 Fjord dynamics and submarine melting in summer

In the *TEMPs* simulations for the summer subglacial discharge, the AW temperature is varied in the same range as in winter. There are several differences to notice between the winter and the summer simulations, apart from the one order of magnitude increase in outflow speed, vertical plume speed and vertically averaged submarine meltrate.

In contrast to the winter case, varying T_{AW} in summer leads to a development through regimes II and III described in Section 3.1.3.2. The $T_{AW} = 4\,^{\circ}\mathrm{C}$ simulation, which is the same as the $Q_{sg} = 4.3\,\mathrm{m^3\,s^{-1}}$ simulation in Section 3.1.3, is characterized by a large-amplitude interfacial wave, submarine melting also in the lower half of the PW layer, and a fast plume being close to having a sufficient buoyancy to reach the surface.

With a cooler AW layer ($T_{AW} = 0\,^{\circ}\mathrm{C}$ and $2\,^{\circ}\mathrm{C}$), the flow is, despite the expected higher buoyancy of the plume due to denser AW, characterized by a smaller-amplitude interfacial wave, plume velocitities similar to the $T_{AW} = 4\,^{\circ}\mathrm{C}$ simulation except in the PW layer, and a vertically averaged meltrate 19.2 % and 36.5 % lower for 2 °C and 0 °C, respectively, than for the 4 °C simulation.

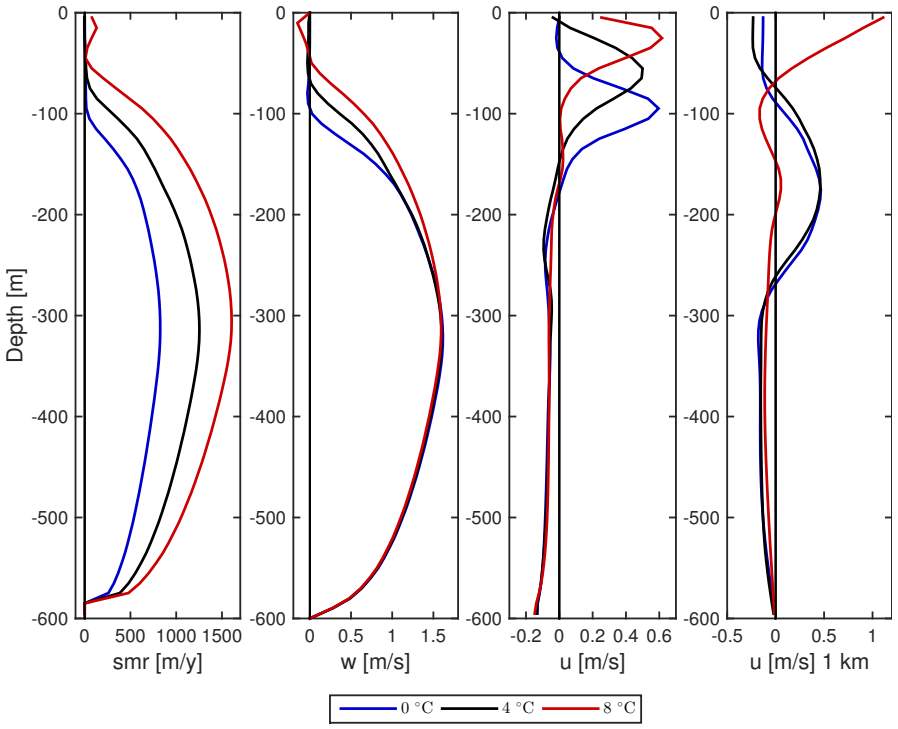

FIGURE 3.9: The effect of variation of AW temperature (0 °C to 8 °C) in summer (*TEMPS*). Vertical profiles of (first) submarine meltrate *smr* [m yr^{-1}], (second) vertical velocity w [m s^{-1}] in the 10 m closest to the glacier front, (third) horizontal velocity u [m s^{-1}] averaged over the 100 m by the glacier front, and (fourth) u [m s^{-1}] 1 km away from the front. All quantities are averaged over a steady state period. Profiles for temperatures 0 °C, 4 °C, and 8 °C are shown.

With a warmer AW layer ($T_{AW} = 6\,°C$ and 8 °C), the plume reaches the surface and sets up a surface outflow of glacially modified water, similar to the simulations with 4 °C AW and a larger subglacial discharge flux. Further away from the glacier front, horizontal velocity profiles reveal a slightly more complex circulation than that in the vicinity of the glacier front (Figure 3.9, fourth panel): The outflow of glacially modified water in the simulations with a warm AW layer occurs in a fast surface current with speed up to 1 m s^{-1}, and in the bottom 400 m, there is a slow and nearly vertically uniform return current of AW towards the glacier front. In addition, there is a return flow within the PW layer confined to about 70 m above the pycnocline. Below the PW return flow, there is a weaker outflow. With warmer AW, the vertically averaged meltrate is higher due to the larger temperature difference between the sea water and the glacier ice, but also due to the increased melting in the PW layer. $T_{AW} = 6\,°C$ and $T_{AW} = 8\,°C$ give a meltrate of 941.9 m yr^{-1} and 1487.1 m yr^{-1}, respectively, which is 22.5 % and 35.7 % higher than for $T_{AW} = 4\,°C$.

3.2 Further studies in deep fjords

3.2.1 Sensitivity of variable subglacial discharge for various AW temperatures – SUMd2

As shown earlier, the submarine melting of a glacer front can be enhanced both by increasing the temperature of the fjord water and by increasing the flux of surface meltwater discharged at depth. As the subglacial discharge varies mostly seasonally and, in contrast, the fjord water temperatures are also controlled by the inflow of water masses from outside the fjord, a large Q_{sg} does not necessarily coincide with a large T_{AW} and vice versa. An example is, during winter, when air temperatures are low and the surface melt is absent, Q_{sg} can be close to zero. At the same time, the fjord water can be relatively warm if the conditions for inflow of external water masses are right.

In *SUMd2*, the aim is to study the sensitivity of the submarine meltrate on the seasonally and atmospherically dependent subglacial discharge for various AW temperatures which are controlled by the water exchange processes with the shelf and the temperature of the off-shore water.

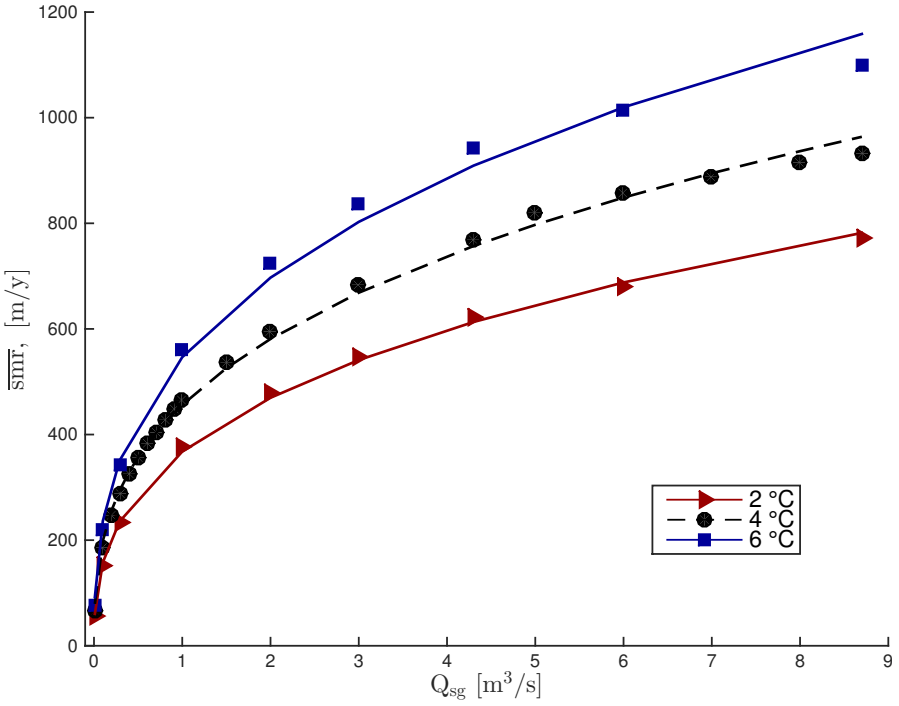

FIGURE 3.10: $\overline{smr}$ as a function of Q_{sg} for AW temperatures of 2 °C (red triangles), 4 °C (black circles), and 6 °C (blue squares). The curves indicate the cubic root fits.

The submarine meltrate increases with the cubic root of subglacial discharge for AW temperatures of 2 °C and 6 °C, as for 4 °C (Section 3.1.3). For a given subglacial discharge in the range 0.01 $m^3 s^{-1}$ to 8.70 $m^3 s^{-1}$, the submarine meltrate increases with increasing

AW temperature in the range explored, like for the winter simulations *TEMP* with $0.01\,\mathrm{m^3\,s^{-1}}$ and summer simulations *TEMPs* with $4.30\,\mathrm{m^3\,s^{-1}}$.

Holding the subglacial discharge flux constant, the difference in submarine meltrate is primarily due to the difference in the temperature of the water entrained in the plume. The *TEMP* and *TEMPs* simulations (Section 3.1.4) show that the plume velocities are dependent on the AW temperature due to the effect the ambient water temperature has on the plume buoyancy. In the winter simulations (*TEMP*) a higher AW temperature leads to a slower plume while in the summer simulations (*TEMPs*), the increased buoyancy from entrained meltwater from the glacier front is larger than the decreased buoyancy in the ambient AW. In this set of simulations, the vertical plume velocity decreases slightly with increasing T_{AW} in the low range of Q_{sg}, in the same manner as in the *TEMP* simulations; and in the high range of Q_{sg}, the plume velocity in the AW layer is less sensitive to changes in T_{AW}. This suggests that the dynamical effect the ambient water temperature has on the plume velocity is negligible, especially for large subglacial discharge fluxes, compared to the direct effect of the temperature difference between the ice and the ambient water driven to the glacier front causing melting at the glacier front.

Common for all AW temperatures is that the vertically averaged vertical plume velocity increases with increasing subglacial discharge and that the ratio of $u_{Q_{sg}}$ to w_{plume} increases with increasing subglacial discharge (a larger percentage of the plume velocity is the discharge velocity for high Q than low).

3.3 Studies of shallower fjords

In this series of experiments, we study the effect of fjord depth and stratification for various subglacial discharge values. The submarine meltrate and fjord circulation in a 200 m deep fjord will be compared to those of the corresponding 600 m deep fjord.

3.3.1 Shallow fjord with thin PW layer – DEPTH

Letting the ratio of the thicknesses of the PW layer and the AW layer be the same for a shallow fjord with depth 200 m and the deep fjord in the previous simulations, i.e.,

$$\frac{H_{PW}}{H_{AW}} = \frac{150\,\mathrm{m}}{450\,\mathrm{m}} = \frac{50\,\mathrm{m}}{150\,\mathrm{m}}, \tag{3.1}$$

we study the effect of the smaller fjord depth on the submarine melting and plume dynamics. We find out whether a smaller depth will inhibit the plume acceleration and thus limit the submarine melting.

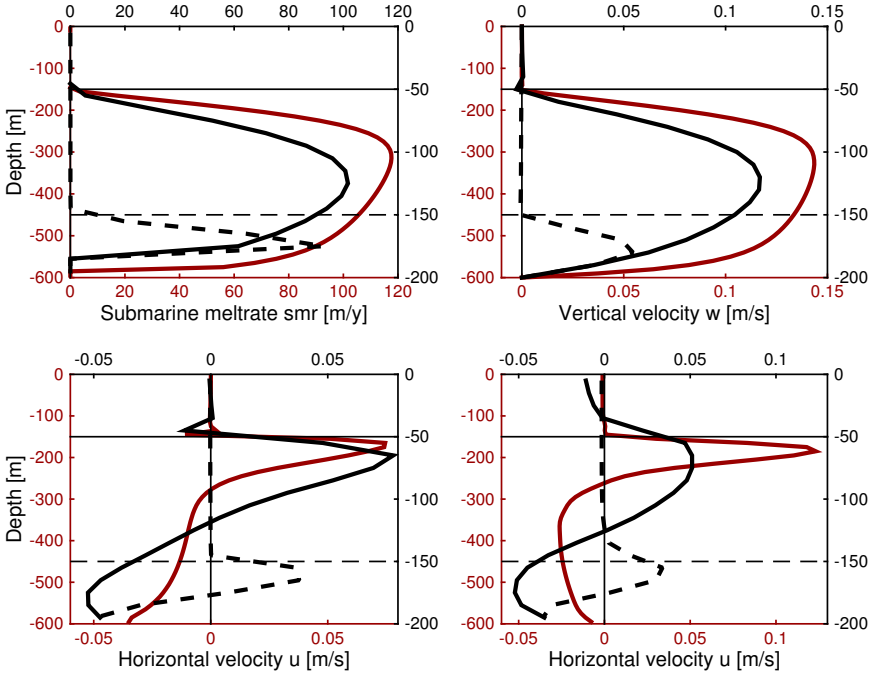

FIGURE 3.11: The effect of variation of fjord depth and layer thickness (*DEPTH* and *PWT*) in winter. Vertical profiles of (upper left) submarine meltrate $smr\,[\mathrm{m\,yr^{-1}}]$, (upper right) vertical velocity $w\,[\mathrm{m\,s^{-1}}]$ in the 10 m closest to the glacier front, (lower left) horizontal velocity $u\,[\mathrm{m\,s^{-1}}]$ averaged over the 100 m by the glacier front, and (lower right) $u\,[\mathrm{m\,s^{-1}}]$ 1 km away from the front. Red curves represent the 600 m deep fjord. Black solid curves represent the shallow (200 m) fjord with 50 m thick PW layer. Black dashed curves represent the shallow (200 m) fjord with 150 m thick PW layer. Thin solid horizontal lines indicate the depth of the interface in the deep fjord (150 m) and in the shallow fjord with thin PW layer (50 m). Thin dashed horizontal lines indicate the depth of the interface in the shallow fjord with thick PW layer (150 m).

In winter, when the subglacial discharge is minimal at $0.01\,\mathrm{m^3\,s^{-1}}$, there are not many differences occuring as a consequence of the different fjord depth. In both fjords, the PW layer acts as a blocking lid for the plume. In the shallow fjord, the vertical plume velocity reaches its maximum values above $0.1\,\mathrm{m\,s^{-1}}$ in the middle of the AW layer, and between the depth of the maximum w and the depth of the interface, the plume slows down and establishes an outflow at the interface (Figure 3.11). This is relatively similar to the corresponding deep fjord winter simulation (*WIN*, Section 3.1.1). Minor differences in the vertical structure and thus the submarine meltrate could be due to the longer vertical distance over which the deep fjord plume may accelerate upwards so that it reaches it maximum w closer to the interface. In the shallow fjord, the PW layer is a third of the thickness of the PW layer in the deep fjord, so its ability to prevent the plume from penetrating the interface is accordingly smaller. However, in the shallow fjord, the plume speed is lower for all depths since the AW layer is shallower, and the

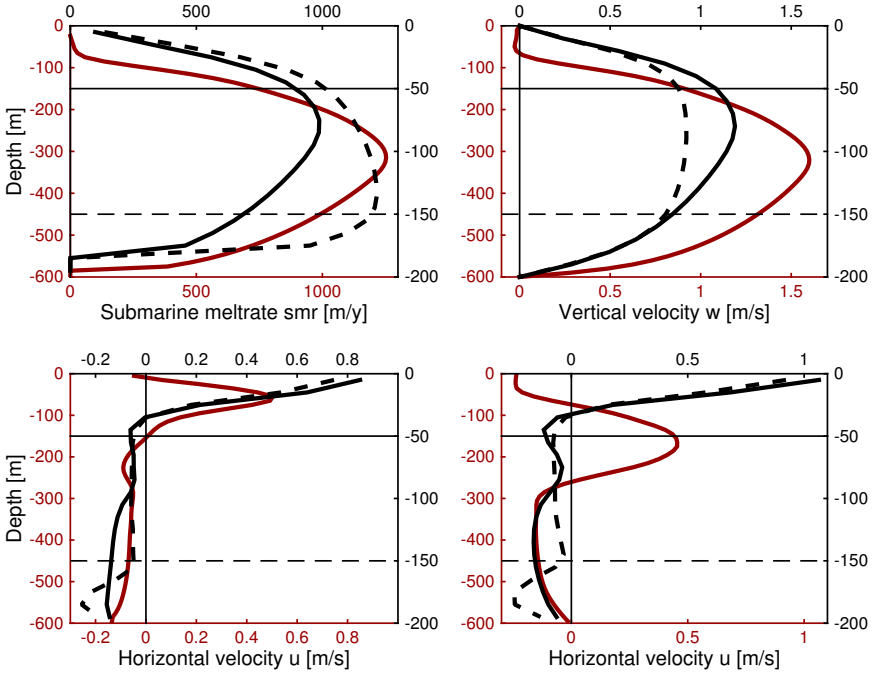

FIGURE 3.12: The effect of variation of fjord depth and layer thickness (*DEPTH* and *PWT*) in summer. Vertical profiles of (upper left) submarine meltrate $smr\,[\mathrm{m\,yr^{-1}}]$, (upper right) vertical velocity $w\,[\mathrm{m\,s^{-1}}]$ in the 10 m closest to the glacier front, (lower left) horizontal velocity $u\,[\mathrm{m\,s^{-1}}]$ averaged over the 100 m by the glacier front, and (lower right) $u\,[\mathrm{m\,s^{-1}}]$ 1 km away from the front. Red curves represent the 600 m deep fjord. Black solid curves represent the shallow (200 m) fjord with 50 m thick PW layer. Black dashed curves and represent the shallow (200 m) fjord with 150 m thick PW layer. Red axes for deep fjord; black axes for shallow fjords. Thin solid horizontal lines indicate the depth of the interface in the deep fjord (150 m) and in the shallow fjord with thin PW layer (50 m). Thin dashed horizontal lines indicate the depth of the interface in the shallow fjord with thick PW layer (150 m).

	$Q_{sg}\,[\mathrm{m^3\,s^{-1}}]$	$H_{PW}\,[\mathrm{m}]$	$H_{AW}\,[\mathrm{m}]$	$\overline{smr}\,[\mathrm{m\,yr^{-1}}]$
WIN	0.01	150	450	67.1
SUM	4.30	150	450	769.0
DEPTH	0.01	50	150	47.9
DEPTH	4.30	50	150	662.1
PWT	0.01	150	50	8.9
PWT	4.30	150	50	895.3

TABLE 3.2: Dependency of fjord depth and layer thicknesses on submarine meltrate.

lower w combined with the overall smaller entrainment of glacial meltwater cause the buoyancy of the plume to be too low for penetrating the PW layer. The vertically averaged meltrate of $47.9\,\mathrm{m\,yr^{-1}}$ is close to that of the deep fjord ($67.1\,\mathrm{m\,yr^{-1}}$).

In summer, however, the depth of the fjord has an impact on the plume dynamics and the submarine melting. The summer plume reaches $1\,\mathrm{m\,s^{-1}}$ mid-depth and continues at that speed until it hits the interface between the layers (Figure 3.12, black solid curves).

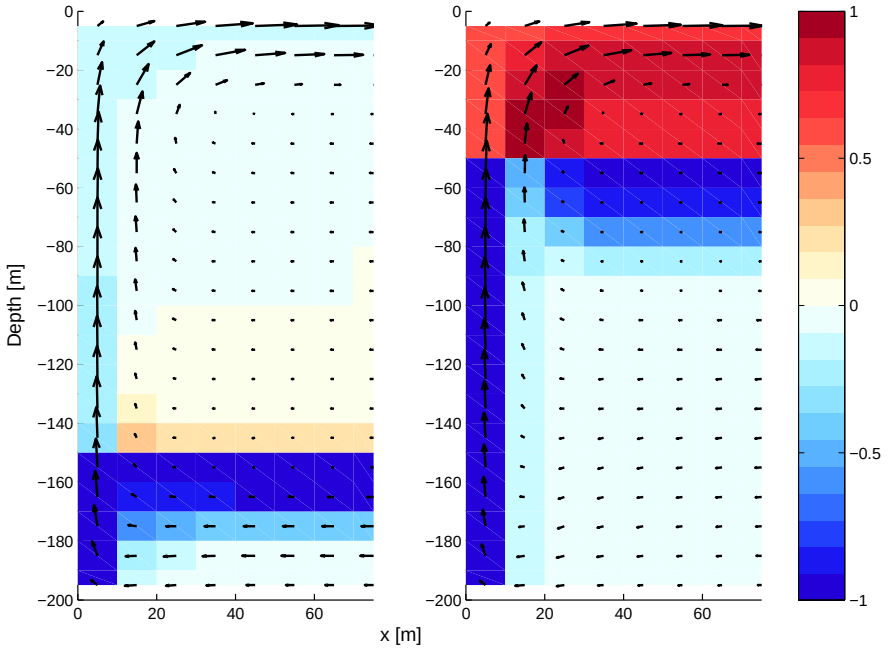

FIGURE 3.13: Fjord current vectors (u, w [$\mathrm{m\,s^{-1}}$]) overlaid salinity anomalies (initial salinity field subtracted from the temporally averaged salinity field) in summer. The PW layer is 150 m (50 m) thick in the left (right) panel. Red (blue) colours represent areas which are more (less) saline than the initially prescribed salinities.

The high vertical speed and rather low density due to the large amount of entrained meltwater from the glacier wall enables the plume to ascend through the PW layer, reach the surface and establish a surface outflow. This differs from the corresponding summer simulation in the deep fjord (Figures 3.9 and 3.12) in which there is a regime II circulation with a large-amplitude interfacial wave and main outflow by the interface.

The vertically integrated submarine meltrate in the AW layer is $42\,892\,\mathrm{m\,yr^{-1}}$ and $10\,669\,\mathrm{m\,yr^{-1}}$ for the deep fjord and shallow fjord, respectively. In other words, within the AW layer, four times as much glacier ice melts in the deep fjord than in the shallow fjord even though the AW layer is just three times as thick in the deep fjord. The salinity anomaly by the glacier front is however larger in the shallow fjord (Figure 3.13, right panel), suggesting that although the shallow-fjord plume melts less (both vertically integrated and vertically averaged over the AW layer), it is more buoyant in the AW layer. For a given subglacial discharge, the buoyancy of the plume at any depth is determined by which entrainment is largest – that of glacial melt or that of ambient AW. As the salinity in the water column by the glacier front in the AW layer is on average 0.5 higher in the deep fjord than in the shallow fjord, the deep-fjord plume entrains more ambient AW as it ascends: The deep-fjord plume ascends faster than the shallow-fjord plume over the entire AW layer (exept right below the interface where its speed is inhibited by the PW layer), and the velocity with which the plume entrains ambient water is assumed to be linearly proportional to the plume velocity. The relatively higher density

of the deep-fjord plume combined with the three times larger ability of the deep-fjord PW layer to block the plume (due to its larger potential energy) causes the difference in circulation and vertical structure of submarine meltrate to differ between the deep fjord and the shallow fjord.

As the shallow-fjord plume reaches the surface, it melts within the PW layer to a greater extent than what the deep-fjord plume does. The shallow-fjord plume melts on average $\overline{smr}_{PW} = 515\,\mathrm{m\,yr^{-1}}$ in the PW layer, while the deep-fjord plume melts only $\overline{smr}_{PW} = 216\,\mathrm{m\,yr^{-1}}$ as it has a decreased vertical speed when it enters the PW layer and its negative buoyancy causes the plume to descend when it has reaches halfway through the PW layer. Overall the submarine meltrates vertically averaged over the entire water columns are $769.0\,\mathrm{m\,yr^{-1}}$ in the deep fjord and $662.1\,\mathrm{m\,yr^{-1}}$ in the shallow fjord.

In addition to the simulations with the winter and summer values of Q_{sg}, two simulations were done in which the subglacial discharge was one and two orders of magnitude, respectively, larger than the winter value, i.e., $0.1\,\mathrm{m^3\,s^{-1}}$ and $1.0\,\mathrm{m^3\,s^{-1}}$. It was found that in the shallow fjord, the $0.1\,\mathrm{m^3\,s^{-1}}$ case leads to a very small overshooting and a following weak wave motion in the upper part of the AW layer limited to the close vicinity to the glacier front, similar to the situation in the deep fjord. For $1.0\,\mathrm{m^3\,s^{-1}}$, the fjord circulation is in regime II in which the overshooting of the interface is large and the glacially modified water flows away from the glacier front along the interfacial wave. Also in the deep fjord, the flow has these features when the subglacial discharge has this magnitude.

3.3.2 Shallow fjord with thick PW layer – PWt

Above, it was shown that the thickness of the capping PW layer can impact the fjord circulation and submarine melting as its thickness determines its capability of blocking the swift plume. Letting the thickness of the PW layer be the same for the shallow fjord of 200 m and the deep fjord of 600 m, i.e., 150 m in both fjords so that the shallow fjord has 50 m thick AW layer below, we examine the impact the total fjord depth and the thickness of the AW layer have on the submarine melting and fjord circulation.

In winter, a circulation is set up in the AW layer as in the deep fjord and the shallow fjord with a thin PW layer. The submarine melting is very limited due to the shallow thickness of the AW layer. The maximum vertical speed of the plume of $0.05\,\mathrm{m\,s^{-1}}$ occurs in the middle of the AW layer where the meltrate reaches its maximum of about $90\,\mathrm{m\,yr^{-1}}$. The vertically averaged meltrate is $8.9\,\mathrm{m\,yr^{-1}}$.

Increasing the subglacial discharge two orders of magnitude from the winter value ($1.0\,\mathrm{m^3\,s^{-1}}$) results in an overshooting of the interface which is slightly larger than in the fjord in which the AW layer is three times thicker. Nevertheless, $\overline{smr}$ is half of that in the shallow fjord with a thinner capping PW layer.

In summer, the vertically averaged submarine meltrate $\overline{smr}$ is $895\,\mathrm{m\,yr^{-1}}$, which is larger than that in the deep fjord with the same capping PW layer and a nine times thicker AW layer ($769\,\mathrm{m\,yr^{-1}}$, Section 3.1.2). It is also larger than in the shallow fjord with a three times thicker AW layer ($662.1\,\mathrm{m\,yr^{-1}}$, Section 3.3.1).

With the summer subglacial discharge, the plume reaches the surface and the fjord gets a regime III circulation, as in shallow fjord with a thin capping PW layer: Within the 50 m thick AW layer, the plume accelerates to $0.8\,\mathrm{m\,s^{-1}}$ before it penetrates the layers' interface and ascends with a speed of up to $0.9\,\mathrm{m\,s^{-1}}$ to the surface. The vertical structure of the plume velocity is essentially the same as for that of the shallow fjord described above, except that in this case, w gets limited as it enters the PW layer at 150 m depth so that this plume has a slightly lower w in the middle 100 m of the fjord. The plume is also slower than that in the deep fjord. The plume in this simulation and the plume in the deep fjord (Section 3.1.2) have approximately the same vertical velocity when they reach the depth of their respective interfaces, but – similar to the other shallow fjord plume (Section 3.3.1) – only the shallow fjord plume reaches the surface due to the difference in w in the AW layer and in the thickness of the AW layer, both having an impact on the total entrainment of dense ambient water into the plume. The large amount of submarine melting in the PW layer in the shallow fjord contributes to making the overall submarine meltrate larger in the 200 m fjord than in the 600 m fjord.

However, there are other processes contributing to making the submarine meltrate large in the shallow fjord with thick capping PW layer. In the previous simulations, the meltrate increases with increasing vertical plume speed and with increasing fjord temperature in the vicinity of the glacier front, and the vertical structure of the meltrate closely resembles that of the vertical plume speed. This is not seen in this fjord: the profile of submarine meltrate has a different shape than that of w (Figure 3.12, upper panels, dashed curves), and in the thick PW fjord, the plume is slower (Figure 3.12, upper right panel, black curves) and the water column is colder (Figure 3.14) than in the thin PW fjord; nevertheless, the overall submarine melting is larger.

Comparing the circulation and temperature distribution in the vicinity of the glacier front in the two shallow fjords with different PW and AW layer thicknesses, we see that the overall circulation is essentially the same. In both fjords, the plume establishes a strong surface outflow confined to the upper 30 m. Regardless of the depth of the

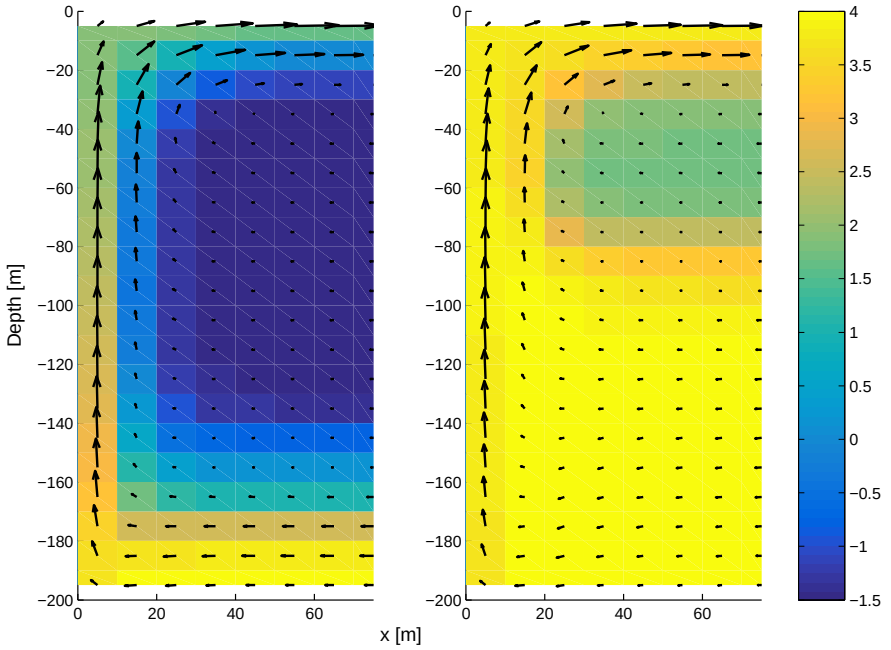

FIGURE 3.14: Fjord current vectors (u, w [$\mathrm{m\,s^{-1}}$]) overlaid temperature (the temporally averaged temperature field). The PW layer is 150 m (50 m) thick in the left (right) panel.

interface between the layers, the return flow occurs over the lowest 150 m (Figure 3.12, lower panels).

In the fjord with the thick AW layer (Section 3.3.1), the return current is close to vertically uniform over the entire AW layer, while in the fjord with the thick PW layer capping a thin AW layer, the return current is strongest in the thin AW layer at the bottom: the return flow in the lower 100 m of the PW layer has an average speed of $0.06\,\mathrm{m\,s^{-1}}$ toward the glacier, while within the AW layer at the bottom, the average speed is three times higher. This difference in the vertical structure of u between the two shallow fjords leads to a difference in the supply of warm ambient AW to the glacier front. In the fjord with a thin AW layer, the return current core along the bottom drives heat to the glacier front close to the bottom, causing a maximum of submarine melting at the depth of the interface at 150 m (Figure 3.12, left panel, dashed curve). The quick renewal of warm water at the glacier front at depth causes a large positive temperature difference relative to the initial temperatures along the enitre depth of the glacier front (Figure 3.15) as the plume brings a large portion of warmer ambient water as it ascends along the glacier. Comparing the 100 m in the vertical which is occupied by PW in the fjord with a thick PW layer and by AW in the fjord with a thin PW layer, we see that the temperature anomaly in the water column in which the plume ascends is much larger in the fjord where this layer is occupied by PW (δT = 3.6 °C to 4.4 °C and T = 2.1 °C to 2.9 °C) (Figure 3.15). This shows that although the AW layer is thin, the relatively faster return current within this layer causes the plume to entrain much

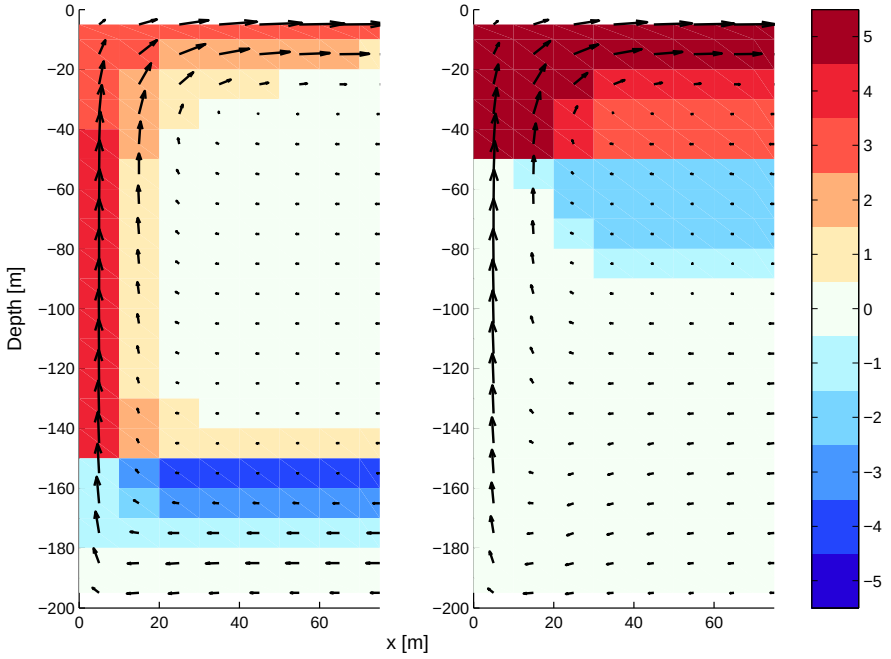

FIGURE 3.15: Fjord current vectors (u, w [$\mathrm{m\,s^{-1}}$]) overlaid temperature anomalies (initial temperature field subtracted from the temporally averaged temperature field). The PW layer is 150 m (50 m) thick in the left (right) panel. Red (blue) colours represent areas which are warmer (colder) than the initially prescribed temperatures.

warm water, melt twice as much glacier ice as in the fjord with a three times thicker AW layer, and bring large amount of extra heat along the glacier front as it ascends.

Even though the temperature anomaly is large and positive in this fjord, in contrast to the negative temperature anomaly in the AW layer in the fjord in which the AW layer is 150 m thick, the water column next to the glacier front is still colder in the thick PW fjord than in the thin PW fjord (Figure 3.14). The water column could be colder due to the larger amount of cold meltwater added to the plume due to the higher meltrate. The water properties in the water column by the glacier front is determed by the entrainment of ambient warm and saline water into the plume on one hand, which causes the plume to become less buoyant, and on the other hand by the addition of cold and fresh meltwater from the melting of glacier ice, which increases the buoyancy of the plume. As the plume in the fjord with the thin AW layer is slower above 150 m than the plume in the fjord with the thick AW layer, the relatively larger amount of entrained saline AW at the bottom could outweigh the effect of the larger amount of entrained fresh meltwater from the glacier front so that the plume is slower than that in the other shallow fjord.

To sum up, in the fjord with the thin AW layer, the jet-like structure in the lower 100 m contributes to a large amount of warm AW being transported toward the glacier front, which results in a large meltrate close to the interface but also acts to limit the

buoyancy and thus the velocity of the plume. In turn, the large meltrate causes a larger entrainment of meltwater into the plume, which limits the temperature increase in the water column by the glacier front but also prevents to some degree the entrained AW to decrease the plume buoyancy.

Chapter 4

Discussion

4.1 Reproduction of fjord dynamics and submarine melting in the Sermilik fjord

4.1.1 Control experiment

The control experiment *WIN* (3.1.1) in this study gives results which in many respects is in good agreement with the results of the MITgcm simulation done by Sciascia et al. (2013). The overall features are the same, and the vertically averaged submarine meltrate are close to equal.

Regarding the fjord circulation, there is a difference between this study and the simulation by Sciascia et al. (2013). We get a single-cell circulation within the AW layer and close to no motion in the PW layer. Sciascia et al. (2013) on the other hand got a double-cell circulation due to the generation of two distinct plumes. Their AW layer circulation is as in this study, and in addition there is a circulation within the PW layer which is generated by melting of the glacier front above the interface. Such a double-cell circulation has been observed in the Sermilik Fjord by Straneo et al. (2011). The velocities of the PW layer plume and the following surface outflow are, however, an order of magnitude smaller than the AW velocities, and the melting in the PW layer is seemingly neglible, causing the overall features of their control experiment and the *WIN* experiment in this study to be quite similar. It should also be mentioned that due to the risk of calving and large amounts of sea ice and and ice bergs close to the glacier make in situ observations of the conditions of the upper layer extremely difficult to obtain with a sufficient quality.

The lack of submarine melting and circulation in the PW layer in this study could be due to differences in the melt rate parameterizations. An initial velocity is required for melting to take place. Therefore must the winter subglacial discharge be larger than zero. Also nonzero values smaller than that chosen as the winter discharge are insufficient to establish the kind of circulation we seek. Very small discharge values – an order or two smaller than $0.01\,\mathrm{m^3\,s^{-1}}$ – lead to some melting close to the meltwater channel at the bottom, but entrainment of ambient AW increases the plume density so quickly that the plume is no longer buoyant and thus does not ascend by the glacier front but instead flows horizontally away along the bottom. It is not known the exact winter-time value of Q_{sg} in Sciascia et al. (2013) and whether their model permitted the generation of an ascending plume solely from melting at the glacier front and in the absense of an initial forced plume.

The fjord currents in the AW layer are generally larger in this study: The speed of the nose of the horizontal outflow current at the interface is about three times larger than in Sciascia et al. (2013). The plume is this study reaches a slightly higher maximum speed below the interface, but also the vertically averaged vertical plume speed is higher due to the quick acceleration in the bottom 50 m in this study. Although the winter subglacial discharge of $0.01\,\mathrm{m^3\,s^{-1}}$ causes an initial plume velocity which is only $5 \times 10^{-5}\,\mathrm{m\,s^{-1}}$ (Equation 2.14) when the discharge exits the meltwater channel, it could be that this initial water motion causes large submarine meltrates already close to the meltwater channel, and that this in turn accelerates the plume to rather high speeds at depth. This could be one of the reasons why the vertical plume velocity and the submarine meltrate vary with depth differently in this study than in Sciascia et al. (2013).

Another contributor to the difference could be the choice of boundary condition at the glacier front. In this study, a free-slip condition is used, and this could allow for a more steep gradient in plume speed up to the maximum which is determined by the density difference between the plume and the PW layer. Sciascia et al. (2013) on the other hand used a no-slip condition on the glacier wall, which could explain the more gradual increase of vertical plume speed toward the interface (nearly constant $\frac{\partial w}{\partial z}$). According to Kimura et al. (2014), the character of the plume and therefore also the meltrate is critically dependent on the boundary conditions at the wall. Observations of the structure of glacier fronts obtained by studying them recently after a calving event (Powell, 2012) show that the glacier front is highly variable. For instance are areas above meltwater channels characterized by half-cylindrical cut-outs made by the ascending plume and helical vortices. In areas where the submarine melting is not forced by subglacial discharge from meltwater channels, there can be a structure which resembles shallow bowls with cusps between them. In addition, the overall structure of the glacier front is affected by other forcings. Thus, it is not obvious how to formulate a

boundary condition that takes the highly variable structure into account. Kimura et al. (2014) shows that the choice of boundary condition does impact the meltrate due to the difference in vertical velocity near the glacier front, and they argue that a no-slip condition should not be used when the boundary layer turbulence is not fully resolved. As the difference between a drag boundary condition and the free-slip condition is small (Kimura et al., 2014), it may be justified to use a free-slip condition if a drag boundary condition is not developed for the model.

4.1.2 AW temperature experiments

4.1.2.1 The relation between AW temperature and submarine meltrate

In the simulations in which the AW temperature varied (3.1.4), we found a linear relation between T_{AW} and $\overline{smr}$ in both winter ($Q_{sg} = 0.01\,\mathrm{m^3\,s^{-1}}$) and summer ($Q_{sg} = 4.3\,\mathrm{m^3\,s^{-1}}$), which is in good agreement with several other modelling studies. Examples include Jenkins (2011) (one-dimensional plume model), Xu et al. (2012) (general circulation model with vertical ice wall), and Sciascia et al. (2013). Xu et al. (2012) argues that a linear dependency of submarine melting on ocean temperature is to be expected when the flow speed of fresh water along the ice face does not increase with respect to the ocean thermal forcing. In this study, the variation in the flow speed of freshwater along the ice face, i.e., the vertical plume speed, was limited to a small decrease with increasing T_{AW} in winter (due to the decreasing plume buoyancy, Figure 3.8) and a small increase near the layers' interface in summer (Figure 3.9). By the argument of Xu et al. (2012) the linear relation found in this study is reasonable. On the other hand, there are also studies that have shown a non-linear relation between the meltrate and the water temperature; a review of previous studies by Holland et al. (2008) states that several experimental and theoretical studies on ice melting in saline water have shown an above-linear increase in meltrate with increasing water temperaure. These are, however, studies of ice shelf basal melting and ice shelf meltwater plumes which govern a range of very low water temperatures, and it is not given that the dependency of submarine meltrate on water temperature is the same for near-freezing temperatures as for the higher temperatures observed in the Sermilik Fjord. Holland et al. (2008) also points out that previous results are obtained with several different assumptions and approaches and that overall, the results are highly variable. Holland et al. (2008) found a quadratic relation by using a three-dimensional general circulation model adapted to the study of cavities beneath ice shelves by Holland and Jenkins (2001).

4.1.2.2 Stability of the water column for high AW temperatures

The density of sea water of the temperatures and salinities most often found in the Arctic is primarily controlled by salinity (Cottier et al., 2010). In the simulations in which the temperature in the AW layer was varied (3.1.4), the density of the cold low-salinity capping PW layer was lower than that of the AW layer regardless of the temperature of the AW. The variation of the AW temperature only caused small density variations of the fjord water, which in winter led to a small decrease of the plume speed as T_{AW} increased as a result of the smaller density difference between the plume and the ambient water. However, for the highest temperatures in the range explored, temperature changes do contribute some to the density of the layer. The stability of the water column for $T_{AW} = 8.0\,°\mathrm{C}$ was marginal, and the weak pycnocline made the water column susceptible to vertical motion even for the rather low vertical plume speed in the *TEMP* (winter) simulation. The increased mixing of cold PW into the AW layer in the vicinity of the glacier front caused the submarine meltrate to be smaller for $T_{AW} = 8\,°\mathrm{C}$ than for $T_{AW} = 7\,°\mathrm{C}$ (3.1.4, Figure 3.7, right panel). The PW layer did not block the plume in the same manner as for lower T_{AW} values, so the plume accelerated further as it ascended and slightly overshot the initial interface and caused some melting above the depths in which the colder plumes melted. The outflow also got lightly elevated compared to the those for colder AW (Figure 3.8), due to the weakened pycnocline.

In summer (the *TEMPs* simulations), the fjord dynamics changed from regime II to III when the AW temperature increased from $4\,°\mathrm{C}$ to $6\,°\mathrm{C}$ and $8\,°\mathrm{C}$, so instead of establishing an interfacial wave, the plume penetrated through the PW layer and set up a surface outflow (Figure 3.9, red curve, right panels). The change of regime due to AW temperature changes does not seem to happen of the same reason as that in the *SUMd* simulations (3.1.3) with varying Q_{sg}. Increasing Q_{sg} leads to a faster ascending plume with more entrained meltwater, while increasing T_{AW} does not increase the plume velocity within the AW layer. Instead, the change from interfacial wave and outflow to PW penetration and surface outflow seem to happen as a result of the density changes: warmer AW has a lower density and therefore makes a smaller density difference between the AW layer and the PW layer (weaker pycnocline), and as more glacier ice melts in warmer AW, more meltwater is entrained in the plume, further decreasing the plume density, making penetration of the PW layer more likely.

4.1.3 Seasonal variation in submarine melting

It was found that the submarine melting varies between winter and summer. The vertically averaged meltrate is one order of magnitude larger in summer than in winter, a

result which was also obtained by Sciascia et al. (2013) using the MITgcm with a similar model setup as in this study.

It was also found that the vertical structure of the meltrate is dependent on the season, mainly due to the magnitude of the subglacial discharge and the vertical plume velocity to which it contributes. The seasonal difference of the vertical structure found in this study was however smaller than that found by Sciascia et al. (2013) who modelled a summer plume which was fast and melted much locally close to the bottom of the fjord and proceeded to slow down and therefore also melt less as it ascended. In contrast, the summer plume in this study accelerated away from the bottom, as in the winter case, though more smoothly in summer than in winter (the winter plume accelerated quickly near the bottom and more slowly middepth, while the summer plume had a more constant increase of w with respect to distance from the bottom). Both in this study and that by Sciascia et al. (2013), the structure of submarine meltrate closely resembles the plume's vertical velocity. Sciascia et al. (2013) explains the increasing smr and w with respect to z in winter with the addition of meltwater being the primary buoyancy forcing on the plume so that as the plume ascends, it entrains more meltwater and thus ascends quicker. This is in agreement with this study. According to Sciascia et al. (2013), the summer plume slows as it ascends along the glacier front because the large summer subglacial discharge at the bottom causes the large buoyancy flux there and that therefore the plume velocity is maximum close to the bottom. However, in this study, the summer subglacial discharge leads to a high meltrate close to the bottom, which in turn adds to the buoyancy of the plume and thus accelerates it further, which in turn causes more melting as the plume ascends.

The difference of the vertical structures of the meltrate could also have to do with the difference in vertical structure of the return current; in this study the return current is rather vertically uniform (Figure 3.9, black curves), while the return current of Sciascia et al. (2013) increases in strength toward the bottom. This is also seen in the shallow fjord simulations with a fjord in which the AW layer is constricted to the lowermost 50 m: the return current has a maximum along the bottom (Figure 3.12, dashed curves) and this is thought to be contributing to the vertical structure of the submarine meltrate (Figure 3.12, upper left panel, dashed curve, 3.3.2), which also decreases with distance from the bottom. It is possible that not only the subglacial discharge and the plume speed but also the vertical structure of the rate of heat transport toward the glacier front could determine at which depths the meltrate is largest.

The values of the subglacial discharge for which the fjord dynamics changes regimes, i.e., from single-cell AW circulation to interfacial wave and outflow between the two layers to single-cell full-fjord circulation with surface outflow, are found to be different in this

study than in Sciascia et al. (2013). In this study, there is especially a tendency of mixing across the interface due to a wave establishing there already for subglacial discharge fluxes in the low range. In contrast, Sciascia et al. (2013) found that the transition between the regimes occurred for larger Q_{sg}. This could be a direct consequence of the different boundary conditions chosen for the rigid boundaries. The velocity of the plume, the outflow current and the return current are generally higher in this study (3.1.1, 3.1.2) than in Sciascia et al. (2013), and the difference seems to increase with increasing subglacial discharge. As the plume velocity increases, the ability of the plume to penetrate the layers' interface increases. This is partly due to the larger plume momentum and partly due to the increased buoyancy as a result of the increased plume velocity which gives more melting and thus more entrained low-density meltwater into the plume. This hypothesis is supported by Kimura et al. (2014) who states that the plume speed by the glacier front and thus the meltrate is critically dependent on the boundary condition.

4.1.4 Sensitivity of various processes on submarine melting

We have shown that the submarine melting – both its vertical mean and its vertical structure – is sensitive to the influx of freshwater at depth and to the heat supply toward the glacier front, i.e., the temperature of the fjord water, the thickness of the warm bottom layer, and the speed of the return current that drives ambient warm water back to the glacier ice as the plume ascends and mixes cold water from the subglacial discharge and submarine melting at the front with the ambient fjord water.

Here, we try to quantify which processes are the primary drivers of submarine melting for given water properties or for a given range of subglacial discharge.

4.1.4.1 Fitted curves and derivatives

The cubic-root dependency of submarine meltrate on subglacial discharge (Figure 3.4) can be described with a function given by

$$\overline{smr}(Q_{sg}) = \left(480.4\,\sqrt[3]{|Q_{sg}|} - 24.25\right)\mathrm{m\,yr^{-1}}. \tag{4.1}$$

with a coefficient of determination of $r^2 = 0.9974$. Here, and in the following equations, the vertical bars denote that one takes the numerical value of the quantity, i.e., without

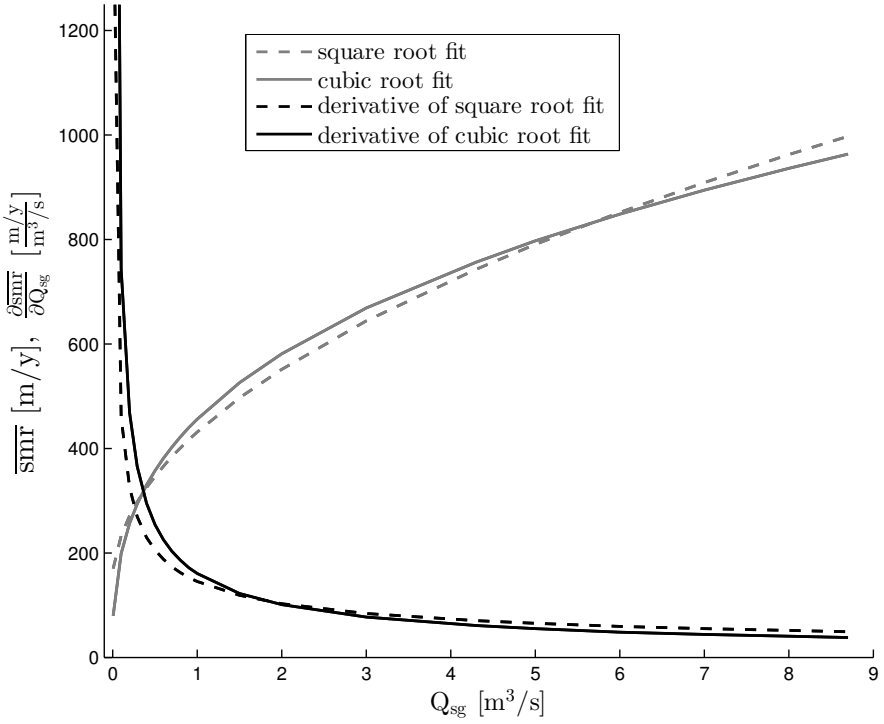

FIGURE 4.1: The dependency of $\overline{smr}$ on subglacial discharge in a fjord with $T_{AW} = 4\,°C$. The solid curves indicate the cubic root fit of $\overline{smr}$ (gray) and its derivative (black), and the dashed curves indicate the square root fit (gray) and its derivative (black).

the unit. The derivative is

$$\frac{\partial\overline{smr}}{\partial Q_{sg}} = \left(160.1\frac{1}{\sqrt[3]{|Q_{sg}|^2}}\right)\frac{\text{m}\,\text{yr}^{-1}}{\text{m}^3\,\text{s}^{-1}}, \tag{4.2}$$

which has rather large values for small values of Q_{sg}, emphasizing the how rather small variations in the subglacial discharge in this range will give large variations in the submarine meltrate (Figure 4.2).

Previous studies (e.g. Sciascia et al., 2013) have found a square root dependency of $\overline{smr}$ on Q_{sg}; in this study, the square root fit has a slightly smaller coefficient of determination $r^2 = 0.9766$, and a function and its derivative given by

$$\overline{smr}(Q_{sg}) = \left(290.3\sqrt{|Q_{sg}|} + 141.2\right)\text{m}\,\text{yr}^{-1} \tag{4.3}$$

and

$$\frac{\partial\overline{smr}}{\partial Q_{sg}} = \left(145.2\,\frac{1}{\sqrt{|Q_{sg}|}}\right)\frac{\text{m}\,\text{yr}^{-1}}{\text{m}^3\,\text{s}^{-1}}, \tag{4.4}$$

respectively, which have similar structures as those for the cubic root fit (Figure 4.1). Therefore, regardless of whether the submarine meltrate has a cubic root or a square

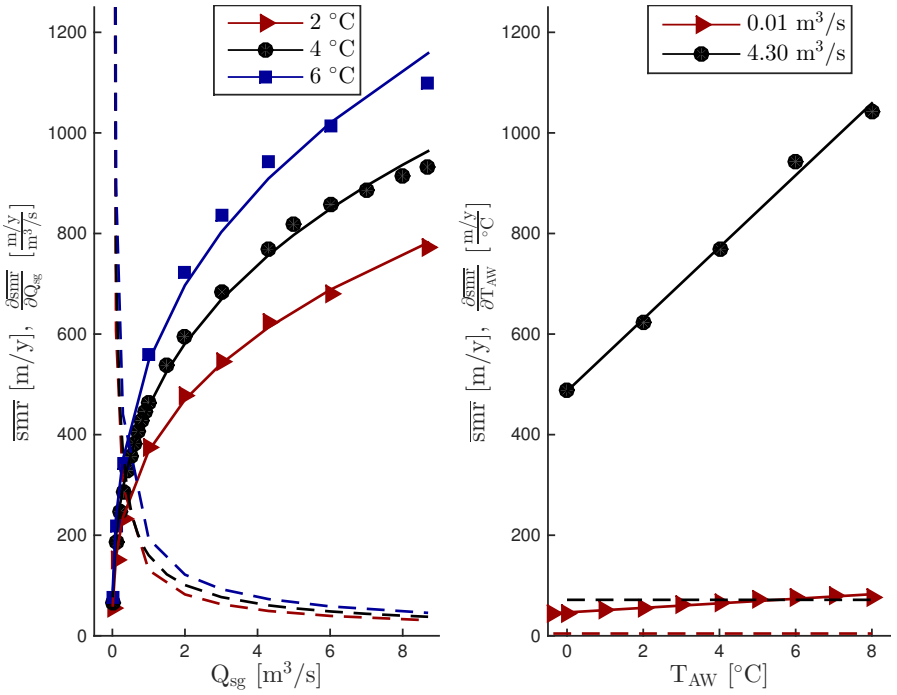

FIGURE 4.2: The dependency of $\overline{smr}$ on subglacial discharge (left) (3.2.1) and on AW temperature (right) (3.1.4). The solid curves in the left panel indicate the cubic root fits of $\overline{smr}$ (right panel: linear fits), and the dashed lines indicate the derivatives of the fitted curves.

root dependency on subglacial discharge, a small increase in Q_{sg}, especially in the range $0\,\mathrm{m^3\,s^{-1}}$ to $1\,\mathrm{m^3\,s^{-1}}$, are likely to result in a large increase in $\overline{smr}$.

If the air temperature would increase, not only would more snow, firn and surface ice melt and enlarge the subglacial discharge and consequently the submarine meltrate in the melting season, but also could the length of the melting season increase so that there would be more weeks in which the surface melt is large.

The amount of glacier ice melted on the glacier front could possibly also be increased to a large extent as a result of a more unstable weather with air temperatures more often increasing above 0 °C. If a larger part of the year gets air temperatures above the freezing temperature, for instance due to more frequent episodes of warm air advection and low pressure systems from south during winter or longer and generally warmer spring and autumn months, time periods which previously had no glacier surface melt and therefore an absence of freshwater discharged in the fjord at depth could now get small amounts of surface melting causing an increase from $0\,\mathrm{m^3\,s^{-1}}$ to a value in the range where the submarine meltrate is highly sensitive to Q_{sg}.

The linear dependency of submarine meltrate on the temperature of the AW layer is given as

$$\overline{smr}(T_{AW}) = \Big(4.5\,|T_{AW}| + 46.5\Big)\,\mathrm{m\,yr^{-1}}, \tag{4.5}$$

and

$$\overline{smr}(T_{AW}) = \Big(5.0\,|T_{AW}| + 45.6\Big)\,\mathrm{m\,yr^{-1}}, \tag{4.6}$$

including $T_{AW} = 8\,^{\circ}\mathrm{C}$ and excluding $T_{AW} = 8\,^{\circ}\mathrm{C}$, respectively, in winter ($Q_{sg} = 0.01\,\mathrm{m^3\,s^{-1}}$). In summer ($Q_{sg} = 4.30\,\mathrm{m^3\,s^{-1}}$), the linear dependency is given as

$$\overline{smr}(T_{AW}) = \Big(71.5\,|T_{AW}| + 486.6\Big)\,\mathrm{m\,yr^{-1}}. \tag{4.7}$$

Since the derivatives of these functions are constant with respect to T_{AW}, the submarine meltrate responds fairly equally to changes in the AW temperature within the range $-0.36\,^{\circ}\mathrm{C}$ to $8.0\,^{\circ}\mathrm{C}$, in contrast to the response to subglacial discharge where the range of Q_{sg} is vital.

In a winter scenario (*WIN* setup with $Q_{sg} = 0.01\,\mathrm{m^3\,s^{-1}}$ and $T_{AW} = 4\,^{\circ}\mathrm{C}$), a $1\,^{\circ}\mathrm{C}$ (25 %) increase of the AW temperature results in a 7 % increase of the submarine meltrate (Equation 4.6). In the same case, a 7 % increase of $\overline{smr}$ due to an increased subglacial discharge would require a 17 % change (Equation 4.1).

With a subglacial discharge of $4.30\,\mathrm{m^3\,s^{-1}}$ (*SUM* setup), increasing T_{AW} from $4\,^{\circ}\mathrm{C}$ to $5\,^{\circ}\mathrm{C}$ results in an 9 % increase of the submarine meltrate (Equation 4.7), which would require the subglacial discharge to increase by 29 %.

In other words, in wintertime when the subglacial discharge is nearly absent, variations in the discharge leads to larger variations in the submarine meltrate than what a corresponding change in the AW temperature would. In summer, however, the AW temperature variations have larger impact on the submarine meltrate.

4.1.5 Are modelled summer meltrates representative for the entire glacier width and throughout the season?

Sutherland and Straneo (2012) estimated a meltrate of $650\,\mathrm{m\,yr^{-1}}$ for the Helheim Glacier using current measurements and hydrographic data from the Sermilik Fjord in summer 2009 to calculate the heat transport toward the glacier. This results is in well agreement with the result of Sciascia et al. (2013) of $738\,\mathrm{m\,yr^{-1}}$ and ours of $769\,\mathrm{m\,yr^{-1}}$. However, as pointed out by Sciascia et al. (2013), one should use caution when comparing the summer meltrates in vertical slices with estimates obtained by calculating the heat transport toward the glacier front. The field-based estimate of the summer meltrate by Sutherland and Straneo (2012) is obtained with data from a few days and is not necessarily representative for the entire summer season. Also, the meltrates obtained in this study and in Sciascia et al. (2013) are obtained with highly idealized simulations which

do not take into account across-fjord variability and the quickly changing shelf–fjord exchange.

4.1.5.1 Fraction of the glacier front characterized by a large subglacial discharge

The rather large submarine meltrates obtained by using large values of subglacial discharge (3.1.3) are probably representative for only portions of the glacier as these rescaled discharge values were obtained by assuming that the surface meltwater would drain through the glacier and be discharged through a single channel. In order to estimate submarine meltrates for the entire width of the glacier in the summer months, it would be incorrect to scale up the submarine meltrate for the 10 m wide model fjord to the width of the real fjord as there are large areas on the glacier front without such large drainage channels. Instead one could try to obtain knowledge about the spatial pattern of subglacial discharge along the glacier width, i.e., an estimate of the number and size of the glacier's drainage channels, and attribute a high meltrate to the area in which large amount of surface meltwater gets discharged into the fjord and lower – for instance winter (low or absent subglacial discharge) month – values of submarine meltrate to the rest of the glacier width. Then the summer-time meltrate averaged over the entire width of the glacier front would be significantly smaller than the values suggested in this study. The summer meltrates obtained in this study are of similar order of magnitude as previous studies (Jenkins, 2011; Sciascia et al., 2013), but across-fjord variations of subglacial discharge were not taken into account in these studies.

Another consideration must be taken into account if one tries to obtain meltrates representative for the entire glacier width. Although a given surface melt volume is discharged through one drainage channel and gives some submarine meltrate value, the same surface meltwater volume discharged through a different number of channels would probably not result in the same total submarine meltrate as there is a non-linear relationship between subglacial discharge and submarine meltrate (3.1.3).

4.1.5.2 Influence of meltwater channel properties

The functional dependence of submarine meltrate on subglacial discharge found in this study and by others (e.g. Jenkins, 2011; Sciascia et al., 2013) is only valid for a given channel geometry. That is, for a given value of subglacial discharge, the submarine meltrate can take a value in a wide possible range depending on the size of the drainage channel where it meets the fjord. Also the thickness and width of the channel has an impact on the meltrate for a given subglacial discharge and channel size; it has been

shown that a thin (vertically) and wide channel results in more melting than a thicker and narrower channel (Kimura et al., 2014).

4.1.5.3 Temporal variation in submarine melting

Subglacial discharge could be intermittent or have a large temporal variability within one summer in addition to being highly variable spatially. Field-based estimates of meltrates are uncertiain (Sciascia et al., 2013), and since field observations are performed in a restricted amount of time, they are not necessarily representative for the entire season. Motyka et al. (2013) investigated the submarine melting of the LeConte Glacier in Alaska and found that the meltrate increased from $9\,\mathrm{m\,d^{-1}}$ to $17\,\mathrm{m\,d^{-1}}$ over a four day period as a result of a strong increase in the subglacial discharge ($130\,\mathrm{m^3\,yr^{-1}}$ to $440\,\mathrm{m^3\,yr^{-1}}$) following a major rainstorm.

4.2 Calving

The presense of a fresh and cold capping layer of PW limits the melting of the glacier front close to the surface by preventing the buoyant plume from ascending past the interface in the case with low subglacial discharge, i.e. in the winter season or during the summer months if the surface meltwater which is drained to the base of the glacier is distributed along a large portion of the glacier width. In time, this leads to a modification of the glacier front; large meltrates middepth and little or limited melting closer to the surface can lead to undercutting and the creation of outward-slanting ice cliffs or ice tounges which is more prone to calving (Motyka et al., 2013).

In the cases where a capping surface layer limits the overall submarine melting and leads to undercutting of the terminus, the modelled vertically averaged meltrates are not necessarily reflecting the ice loss due to submarine melting but are rather underestimating the ice loss as it is likely that persistent undercutting increases the calving rate and thus the ice loss. Underestimation of the ice loss provide an uncertainty in predictions of the future sea-level rise and should therefore be taken into account. Submarine melting at the glacier front as a driver of calving has been discussed by several (e.g. O'Leary and Christoffersen, 2013; Vieli et al., 2002), but there are few detailed studies of changes in the near-terminus velocity and changes in the submarine meltrate (Andersen et al., 2010). O'Leary and Christoffersen (2013) modelled static stress fields in idealized tidewater glaciers to study the effect undercutting due to inhomogeneous submarine melting has on calving and found that the undercutting can drive calving at up to ten times the mean meltrate. This indicates that if the goal is to estimate the total ice loss from

the glacier terminus due to submarine melting, the vertical structure of the submarine meltrate – in addition to vertical means – should be taken into consideration as it is likely to have a large impact on the calving rate.

4.3 The effect of fjord depth and stratification

In Sections 3.3.1 and 3.3.2 we investigate the fjord circulation and submarine melting in 200 m deep fjords in order to ascertain that this approach is suitable also for shallower fjords than the Sermilik Fjord in Greenland. We find that the depth of the fjord is an important factor for the submarine meltrate and fjord circulation in several aspects.

In a fjord where the stratification is the same as in a deeper fjord, the layers in the shallow fjord are thinner (Section 3.3.1). First of all, this causes the capping upper layer to have a poorer ability to block the plume from penetrating through it and hence may lead to more mixing across the interface. The reduced thickness of the capping layer causes the potential energy to be accordingly smaller, and therefore it has a lower ability of blocking a high-velocity plume. This effect is partially counteracted by the effect of a thinner lower layer. As the lower layer also is thinner, it provides a smaller vertical distance over which the plume can melt glacier ice at the front and entrain ambient warm fjord water. We find that for the summer subglacial discharge value of $4.3\,\mathrm{m^3\,s^{-1}}$, the decreased amount of entrained dense water in the AW layer leads to a regime III type of circulation with surface outflow in the shallow fjord, compared to the regime II type with interfacial outflow in the deep fjord.

We also showed that the stratification in a shallow fjord can have an even larger impact on the meltrate and fjord dynamics (Section 3.3.2). By letting the thickness of the capping layer be the same as that on the deep fjord, we find that the winter meltrate and plume velocity are – not unexpectedly – greatly reduced due to the limited heat supply to the glacier front by the thin lower layer of AW.

However, in summer, the vertically averaged meltrate is discovered to be larger than in both the shallow fjord with a thicker AW layer and the deep fjord. This is unexpected considering our earlier results for several reasons. In the shallow fjord with a thick capping PW layer, the meltrate is larger at all depths than in the shallow fjord with a thin PW layer even though the glacier front in the latter fjord has a three times larger contact area with the warm AW. Earlier results have also shown that the meltrate increases with increasing plume velocity. This is not seen in the comparison between the two shallow fjords of different layer thicknesses; the fjord with the slowest plume has the largest meltrate (Figure 3.12, upper panels, black curves). Our earlier simulations and

the simulations of Sciascia et al. (2013) have shown that the meltrate generally increases with increasing AW temperature, increasing AW layer thickness and plume velocity at the glacier front. The profiles of meltrate and those of vertical velocity at the glacier front generally have similar shape (Figures 3.12, upper panels) due to the effect of larger entrainment of warm ambient water with larger plume speed. Neither this is found in the shallow fjord with a thick capping PW layer. We explain this anomalous results by the difference in the vertical structure of the return current (Section 3.3.2; Figure 3.12, lower panels). The jet-like structure in the shallow fjord capped by a thick PW layer leads large amounts of heat to the glacier front near the bottom, causing high meltrates there.

The freshening of the upper layer by the upwelling at the glacier front is only found in this fjord; in all the other fjords, the buoyant plumes have entrained more saline AW than the overall freshwater addition from the subglacial discharge and submarine melting at the front and thus lead to a more saline capping PW layer. In the fjord with a thick PW layer, the strong return current at depth transports large amounts of ambient warm and saline AW toward the glacier front and the plume, but as the meltrate is very large around the interface of the layers, it is added sufficiently fresh meltwater relative to the entrained saline water to lead a buoyant current of fresher water to the surface.

This example shows the complex interaction between the various processes taking place in the near vicinity of the glacier front. It highlights that the meltrate profiles do not necessarily resemble those of the plume velocity and that a low area of contact between the glacier front and the warm fjord water does not necessarily reduce the meltrate.

Chapter 5

Summary and outlook

A high-resolution non-hydrostatic general circulation model is used to study the buoyancy-driven circulation near a marine-termining glacier front and the submarine melting resulting from oceanic thermal forcing and plume dynamics. We use an idealized setup with flat bathymetry, absence of external forcing from tides and the atmosphere, and non-rotational dynamics to isolate the effect of the presence of the glacier front in the fjord and the resulting submarine melting and fjord circulation. One goal is to reproduce earlier results from simulations of the Helheim Glacier–Sermilik Fjord system in south-east Greenland. Another aim is to gain knowledge abouth whether this approach is applicable to other glacial fjord systems with different fjord depths and water stratifications. In a two-layer stratification with warm and saline water of Atlantic origin at the bottom capped by a fresher and colder Polar Water layer, we examine the variability of the submarine melting and the buoyancy-driven circulation by changing the fjord temperature and the subglacial discharge flux.

Our results indicate that the plume dynamics and submarine melting driven by the presense of the glacier terminus and by the addition of surface meltwater at depth establishes a circulation which on one hand transports glacially modified waters away from the glacier front at either surface level or at the pycnocline separating the water masses in the two layer system, and on the other hand drives a return current of ambient warm and saline fjord water at depth toward the glacier front, replenishing available heat to melt ice.

The depth at which the outflow of glacially modified water occur is primarily controlled by the flux of subglacial discharge. The absence of subglacial discharge in winter leads to a single-cell circulation within the Atlantic Water layer and outflow right below the pycnocline. For large discharge values in summer, approximately $5\,\mathrm{m}^3\,\mathrm{s}^{-1}$ and larger, the plume has a buoyancy which is sufficient to reach the surface and establish an outflow

there. The temperature of the Atlantic Water layer may be a secondary control of the type of circulation. By warming the lower layer by two degrees, a surface outflow was established for the baseline summer discharge flux due to the weakened pycnoline and increased plume buoyancy resulting from the increased entrained meltwater.

We find that there is a large seasonal variability in the meltrate, which is due to the subglacial discharge. In winter, there is little or no snow and firn melting on the surface of the glacier, and thus the subglacial discharge is absent or minor. Thus, the submarine melting of the glacier front is due solely to the presence of warm fjord water and the limited buoyant current along the glacier front. In summer, the surface melt leads to large volumes of freshwater being discharged into the fjord at depth. This sets up a forced plume which leads to higher velocities at the glacier front, more entrainment of ambient warm fjord water and thus a higher meltrate. In our simulations, the summer meltrate is an order of magnitude larger than in winter.

Overall, BOM reproduces the results of the idealized two-dimensional simulations with MITgcm of Sciascia et al. (2013) quite well. We find that the submarine meltrate increases with the cubic-root of subglacial discharge, a relation which is very close to that found by Sciascia et al. (2013). The submarine meltrate also responds to the oceanic forcing; it increases linearly with increasing temperature in the layer of Atlantic Water. Although BOM gives results quite similar to MITgcm, the differences in the meltrate are found to be largest in the cases where the forcings are low, i.e., for rather cold fjord water and for the low range of subglacial discharge.

Our main results are in agreement with several other studies which have investigated the submarine melting of and plume dynamics by glacier fronts. These include one-dimensional plume models (e.g. Jenkins, 2011), two-dimensional vertical slice domains of a GCM with an ice melt model included (e.g. Sciascia et al., 2013), and three-dimensional approaches (e.g. Cowton et al., 2015; Kimura et al., 2014; Xu et al., 2013). There are several functional dependencies between subglacial discharge and submarine melting and between fjord temperature and submarine melting proposed, but over the ranges of subglacial discharge and fjord temperatures studied here, the difference between these dependencies are not very large. For instance does the linear relation between meltrate and fjord temperature found in this study not deviate much from weak quadratic or slightly above-linear relations found in some studies, and the exact dependencies have been shown to vary with the type of study performed (Holland et al., 2008). The cubic-root dependency of meltrate on subglacial discharge found in this study agrees with that found by Jenkins (2011); Xu et al. (2012) but also can also be described almost equally well with a square-root curve (Section 4.1.4.1), which was the dependency found by Sciascia et al. (2013). Similar for most is that the meltrate quickly increases with

increasing subglacial discharge in the low range of discharge values and that the rate of increase decreases as the discharge moves into a higher range.

We have shown that the choice of boundary condition at the rigid boundaries are likely to have an effect on the plume velocity and the submarine meltrate. With a setup of BOM as similar as possible to that of MITgcm with the exception of the boundary condition, the fjord circulation in the vicinity of the glacier front is generally quicker in BOM with a free-slip condition than in MITgcm with a no-slip condition, and this leads to higher meltrates.

Regarding the shallow fjord simulations, we find that our approach is promising for the further development of modelling plume dynamics and submarine melting in a more complex model domain. In winter, the stratification is essential for the submarine melting as the limited thickness of the warm layer serves as a restriction to the ascending plume. The shallow fjord is more sensitive than the deep fjord to subglacial discharge; penetration of the upper layer and a resulting outflow at the surface is more easily established in the shallow fjord. Depending on the stratification, the addition of glacially modified water with entrained Atlantic Water from the lower layer into the upper layer will lead to either more saline water – as found in previous studies – or a freshening of the upper layer. Furthermore, it is found that in shallow fjords with a thin warm bottom layer and thus a restricted heat supply to the glacier front, the meltrate may still be as high as in fjords where a much larger part of the glacier front has contact to warm fjord water. This perhaps surprising result is assumed to be due to faster replenishment of warm ambient water toward the glacier.

We have discussed the importance of including an across-fjord variability of subglacial discharge in future three-dimensional modelling of this circulation. As it is not likely that the surface meltwater volume is uniformly discharged along the entire glacier width, one needs an estimation of the number and size of meltwater channels on the glacier front to correctly distribute the meltwater volume over the channels and thus get probable discharge velocities and fluxes. The submarine meltrate is highly sensitive to the plume velocity, and the velocity with which the subglacial discharge enter the fjord is a primary contributor to the velocity along the glacier front. As proposed by Sciascia et al. (2013), one could assume that a certain portion of the glacier width is characterized by high meltrates resulting from subglacial discharge and high plume velocities, while the remaining parts of the glacier front has meltrates arising from the contact with warm fjord water as in the winter control simulation.

List of References

Andersen, M. L., Larsen, T. B., Nettles, M., Elosegui, P., van As, D., Hamilton, G. S., Stearns, L. A., Davis, J. L., Ahlstrøm, G., de Juan, J., Ekstrøm, G., Stenseng, L., Khan, S. A., Forsberg, R., and Dahl-Jensen, D. (2010). Spatial and temporal melt variability at Helheim Glacier, East Greenland, and its effect on ice dynamics. *Journal of Geophysical Research*, 115(F4).

Bergen Ocean Model (2014). `http://www.mi.uib.no/BOM/`, Accessed: 2015-05-26.

Berntsen, J. (2000). Users guide for a modesplit σ-coordinate numerical ocean model. *Technical Report*, 1:5.

Cottier, F. R., Nilsen, F., Skogseth, R., Tverberg, V., Skarðhamar, J., and Svendsen, H. (2010). Arctic fjords: a review of the oceanographic environment and dominant physical processes. *Geological Society, London, Special Publications*, 344:35–50.

Cowton, T. R., Slater, D. A., Nienow, P. W., Goldberg, D. N., and Sole, A. J. (2015). Effect of near-terminus subglacial hydrology on tidewater glacier submarine melt rates. *Geophysical Research Letters*.

Hellmer, H. and Olbers, D. (1989). A two-dimensional model for the thermohaline circulation under an ice shelf. *Antarctic Science*, 1(4):325–336.

Holland, D. M. and Jenkins, A. (1999). Modeling thermodynamic ice-ocean interactions at the base of an ice shelf. *Journal of Physical Oceanography*, 29(8):1787–1800.

Holland, D. M. and Jenkins, A. (2001). Adaptation of an isopycnic coordinate ocean model for the study of circulation beneath ice shelves. *Monthly Weather Review*, 129(8):1905–1927.

Holland, P. R., Jenkins, A., and Holland, D. M. (2008). The response of ice shelf basal melting to variations in ocean temperature. *Journal of Climate*, 21(11):2558–2572.

Howat, I. M., Joughin, I., and Scambos, T. A. (2007). Rapid changes in ice discharge from Greenland outlet glaciers. *Science*, 315(5818):1559–1561.

Inall, M. E., Murray, T., Cottier, F. R., Scharrer, K., Boyd, T. J., Heywood, K. J., and Bevan, S. L. (2014). Oceanic heat delivery via Kangerdlugssuaq Fjord to the south-east Greenland ice sheet. *Journal of Geophysical Research: Oceans*, 119(2):631–645.

Jackson, R. H., Straneo, F., and Sutherland, D. A. (2014). Externally forced fluctuations in ocean temperature at Greenland glaciers in non-summer months. *Nature Geoscience*, 7(7):503–508.

Jenkins, A. (2011). Convection-driven melting near the grounding lines of ice shelves and tidewater glaciers. *Journal of physical oceanography*, 41(12):2279–2294.

Jenkins, A., Nicholls, K. W., and Corr, H. F. J. (2010). Observation and parameterization of ablation at the base of Ronne ice shelf, Antarctica. *Journal of Physical Oceanography*, 40(10):2298–2312.

Kimura, S., Holland, P. R., Jenkins, A., and Piggott, M. (2014). The effect of meltwater plumes on the melting of a vertical glacier face. *Journal of Physical Oceanography*, 44(12):3099–3117.

Moon, T., Joughin, I., Smith, B., and Howat, I. M. (2012). 21st-Century evolution of Greenland outlet glaciers velocities. *Science*, 336(6081):576–578.

Motyka, R. J., Dryer, W. P., Amundson, J., Truffer, M., and Fahnestock, M. (2013). Rapid submarine melting driven by subglacial discharge, LeConte Glacier, Alaska. *Geophysical Research Letters*, 40(19):5153–5158.

Motyka, R. J., Hunter, L., Echelmeyer, K. A., and Connor, C. (2003). Submarine melting at the terminus of a temperate glacier, LeConte Glacier, Alaska. *Annals of Glaciology*, 36(1):157–65.

O'Leary, M. and Christoffersen, P. (2013). Calving on tidewater glaciers amplified by submarine frontal melting. *The Cryosphere*, 7(1):119–128.

Powell, R. (2012). Estimates of marine tidewater terminus melting in Svalbard. In *IGS symposium, Fairbanks, Alaska*.

Rignot, E., Koppes, M., and Velicogna, I. (2010). Rapid submarine melting of the calving faces of West Greenland glaciers. *Nature Geoscience*, 3:187–191.

Sciascia, R., Straneo, F., Cenedese, C., and Heimbach, P. (2013). Seasonal variability of submarine melt rate and circulation in an East Greenland fjord. *Journal of Geophysical Research: Oceans*, 118:2492–2506.

Straneo, F., Curry, R. G., Sutherland, D. A., Hamilton, G. S., Cenedese, C., Vage, K., and Stearns, L. A. (2011). Impact of fjord dynamics and glacial runoff on the circulation near Helheim Glacier. *Nature Geoscience*, 4(5):322–327.

Straneo, F., Hamilton, G. S., Sutherland, D. A., Stearns, L. A., Davidson, F., Hammill, M. O., Stenson, G. B., and Rosing-Asvid, A. (2010). Rapid circulation of warm subtropical water in a major glacial fjord in East Greenland. *Nature Geoscience*, 3(3):182–186.

Straneo, F. and Heimbach, P. (2013). North Atlantic warming and the retreat of Greenland's outlet glaciers. *Nature*, 504(7478):36–43.

Straneo, F., Heimbach, P., Sergienko, O., Hamilton, G., Catania, G., Griffies, S., Hallberg, R., Jenkins, A., Joughin, I., Motyka, R., Pfeffer, W. T., Price, S. F., Rignot, E., Scambos, T., Truffer, M., and Vieli, A. (2013). Challenges to understanding the dynamic response of Greenland's marine terminating glaciers to oceanic and atmospheric forcing. *Bulletin of the American Meteorological Society*, 94(8):1131–1144.

Sutherland, D. A. and Straneo, F. (2012). Estimating ocean heat transports and submarine melt rates in Sermilik Fjord, Greenland, using lowered acoustic Doppler current profiler (LADCP) velocity profiles. *Annals of Glaciology*, 53(60):50–58.

Vieli, A., Jania, J., and Kolondra, L. (2002). The retreat of a tidewater glacier: observations and model calculations on Hansbreen, Spitsbergen. *Journal of Glaciology*, 48(163):592–600.

Xu, Y., Rignot, E., Fanty, I., Menemenlis, D., and Flexas, M. M. (2013). Subaqueous melting of Store Glacier, west Greenland from three-dimensional, high-resolution numerical modeling and ocean observations. *Geophysical Research Letters*, 40(17):4648–4653.

Xu, Y., Rignot, E., Menemenlis, D., and Koppes, M. (2012). Numerical experiments on subaqueous melting of Greenland tidewater glaciers in response to ocean warming and enhanced subglacial discharge. *Annals of Glaciology*, 53(60):229–234.